AN EXPERIMENTAL STUDY OF THE SEPARATED FLOW FIELD ABOUT SLENDER DELTA WINGS OF TRIANGULAR CROSS SECTION

Thesis by

Hans Werner Grellmann

In Partial Fulfillment of the Requirements

for the Degree of

Aeronautical Engineer

California Institute of Technology

Pasadena, California

1964

(Submitted May 8, 1964)

ACKNOWLEDGEMENTS

The author wishes to thank Professor Peter B. Lissaman whose helpful guidance and criticism made this work possible. Thanks are due to Mrs. Elizabeth Fox for typing the manuscript.

ABSTRACT

The separated flow about slender delta wings of shallow triangular cross section is investigated. The Brown and Michael theory is extended for this cross section and the solution is indicated. The limitations of this theory are pointed out. Computation becomes very complex and other methods such as electrostatic analog procedures appear preferable.

Wind-tunnel tests were carried out on four delta wings with apex angle of 30° and triangular spanwise cross sections with flat base surfaces and included angles at the leading edges of 0, 10, 20, 30°, respectively. These tests were done in the 10-ft. GALCIT low-speed wind tunnel.

Pressure measurements were taken at speeds up to 160 ft./sec. and Reynolds numbers up to 4×10^6 based on the maximum chord of 4 ft. Experimental spanwise pressure distributions are compared to theoretical results for a delta wing of zero thickness (due to Brown and Michael). Experimental results show secondary vortices near the leading edges. These are not taken into account in the theory and so the theoretical and experimental pressure distributions differ markedly.

However, the experimental spanwise local lift coefficient, which is obtained by integrating the spanwise pressure distribution, does agree very well with theoretical results. A simple geometrical definition for a corrected angle of attack makes it possible to plot local lift coefficients for the four wings on one curve.

It is shown that the drag of the wings with triangular cross section including base drag is higher than that for wings of zero thickness. The results are applied to a brief analysis of the possibility of reducing lift-dependent drag of slender delta wings. It is shown that this drag reduction can be substantial (more than 10%) for certain special cross sectional shapes.

TABLE OF CONTENTS

I. INTRODUCTION

Present development of aircraft and space vehicles indicates that in the not too distant future aircraft will operate at hypersonic speeds, and reusable aerospace planes capable of re-entering the earth's atmosphere will be an economic necessity if continued and expanded exploration of space is to be feasible.

These requirements point to the development of highly swept wings, of which the slender delta wing is, for structural and other reasons, the soundest choice. It may become desirable, and this is being investigated at present in the lifting body concept, to use the delta wing not only for its lifting properties but also to improve the aerodynamic properties of the wing-fuselage combination, by giving the wing a thick cross section and using it to store fuel, cargo, and powerplants. The purpose of this research was to gain an understanding of the separated flow field behind such a thick delta wing at moderate angles of attack.

It is well known that the vortex sheets being shed continuously from the leading edges of sharp-nosed slender wings coil up into the form of conical spirals (Ref. 2) which lie just above the wing and determine to a large extent the flow above it. Behind the wing these spiral vortex sheets roll up into the conventional trailing vortices.

The outward flow in the boundary layer on the upper surface of the wing between the point directly below the main vortex core and the leading edge encounters rising pressure gradient and separates forming one or more small vortices near the leading edge. (Ref. 2)

Below each main vortex there is a region of very low pressure. It has been suggested and experimentally verified by G. H. Lee (Ref. 3) in 1959 that this low pressure region may be used to good advantage. If the wing is given an appropriately contoured cross section (see Fig. 4) the lift vector is tilted forward causing a reduction in drag below that of a flat wing of zero thickness.

To solve the problem of separated flow over a slender delta wing theoretically, the flow field is commonly approximated by simplified mathematical models which, to make the problem tractable, neglect the boundary layer separation on the wing and consider only the main vortex sheets in more or less realistic approximations to the real flow.

One such simplified model, due to Brown and Michael (Ref. 1), is used in this study to show how the potential flow over a delta wing of triangular cross section with two concentrated vortices above the wing may be solved in principle. The mathematics becomes rather unwieldy even for this simple cross section and a solution would be prohibitively complex for more complicated shapes. In that case a more promising approach might be the use of an electrostatic analog like a field plotter.

For practical applications, it would be very convenient if pressure distributions for wings of zero thickness could be applied to flat moderately thick wings with sharp leading edges without modification. Making this assumption, some calculations were carried out in this study to show that substantial reduction of lift-dependent drag is possible under certain conditions.

The wind-tunnel tests were carried out on wings with shallow triangular cross sections. This simple cross section was chosen for its structural simplicity and so as not to confuse the issue by introducing too many variables.

II. THEORETICAL CONSIDERATIONS

The problem to be considered is the flow over a slender delta wing with leading edge separation.

The equation for a slightly perturbed compressible flow is, (Ref. 4)

$$(1-M^2)\frac{\partial^2\phi}{\partial s^2}+\frac{\partial^2\phi}{\partial x^2}+\frac{\partial^2\phi}{\partial y^2}=0 \qquad (1)$$

where ϕ is the perturbation potential and the s,x,y coordinates are fixed on the wing as shown in Fig. 1.

Now if we consider very slender delta wings, then $\frac{\partial^2\phi}{\partial s^2}$ will be much smaller than $\frac{\partial^2\phi}{\partial x^2}$ and $\frac{\partial^2\phi}{\partial y^2}$ and thus the first term of equation 1 may be neglected as long as M is not too large. Then we have the equation

$$\frac{\partial^2\phi}{\partial x^2}+\frac{\partial^2\phi}{\partial y^2}=0$$

which is the Laplace equation for the disturbance potential of the two-dimensional crossflow in the x,y plane.

Therefore we see that as long as the term $(1-M^2)\frac{\partial^2\phi}{\partial s^2}$ can be neglected, the three-dimensional flow may be split up into the flow parallel to the wing and the potential crossflow in the plane normal to the wing.

The results obtained by solving for the potential in this way are applicable for both subsonic and supersonic flow (Ref. 5) as long as $(1-M^2)\frac{\partial^2\phi}{\partial s^2}$ is small. In the subsonic case the problem solved is the potential flow over an infinitely long slender delta

wing since the presence of a trailing edge would affect the flow everywhere. A finite wing in subsonic flow will not produce the conical flow field which results from the slender body theory.

But in the supersonic case there is no upstream influence and a shock wave will terminate the flow field over the upper surface of a finite wing at a positive angle of attack and therefore that flow field is conical and can be predicted right up to the trailing edge from the slender body theory.

A. Flat Wings

The potential flow about a slender flat delta wing of zero thickness with leading edge separation has been solved by Brown and Michael (Ref. 1), using the slender body theory and a mathematical model of two concentrated vortices above the wing connected to the leading edges by plane vortex sheets. The spiral vortex sheets in the real flow are thus approximated by placing concentrated vortices near the center of the coiled up sheets and since the vortices grow in strength with s, the plane vortex sheets from the leading edges supply the necessary vorticity increase with s.

The boundary conditions at the wing are (1) that the normal velocity component must vanish and (2) that there is no flow around the sharp leading edge. This is analogous to the Kutta condition normally applied at trailing edges of wings.

The condition applied in the flow field is that the net force acting on the combined system of concentrated vortex and vortex sheet be zero.

A solution to the Laplace equation satisfying the above-mentioned conditions can be found numerically and from the resulting complex velocity potential the pressure at the surface of the wing can be found, taking into account also the flow component parallel to the wing surface.

Strictly speaking this is not correct, of course, since both the strength of the main vortices and their height above the wing increase with s. The approximation is suitable however for wings of extremely small apex angle and at very small angles of attack in which case the vortices appear as two dimensional in the x,y plane. This mathematical model does not consider real effects but gives good results for overall lift coefficient, while not succeeding in predicting the spanwise pressure distribution across the wing. The results of Brown and Michael are compared to the experimental results in Figs. 19, 20, 22.

B. Wings of Triangular Cross Section

The method may be extended to slender delta wings of triangular cross section, as illustrated in Fig. 1.

Consider two complex planes z and ζ, where $z = x + iy$, $\zeta = \xi + i\eta$, as shown in Fig. 2. The wing cross section is located in the z-plane with the vertex of the triangle at the origin and the imaginary axis bisecting the triangle. By symmetry we may consider the flow in the half-plane $x > 0$ independently. We now wish to transform the half-plane $x > 0$ bounded by the imaginary axis and the lines AB and BC in the z-plane to the half-plane bounded

by the imaginary axis in the ζ-plane. The triangle is thus transformed into a straight line. The transformation $z = f(\zeta)$ is

$$z = A \int_{+i}^{\zeta} \left(\frac{\zeta}{\zeta - i}\right)^{\beta} \left(\frac{\zeta}{\zeta + ic}\right)^{\frac{1}{2}} d\zeta$$

where A is a constant and $2\beta\pi$ is the vertex angle of the triangle. The constant c determines η for the point C.

In the ζ-plane, we have a free stream $U\alpha$ in the η direction and two vortices at ζ_o and $-\overline{\zeta}_o$. Thus the velocity potential for the flow in the ζ-plane is

$$F(\zeta) = -i \frac{\gamma}{2\pi} \ell n \left(\frac{\zeta - \zeta_o}{\zeta + \overline{\zeta}_o}\right) - i U \alpha \zeta$$

where γ is the strength of the vortex at ζ_o.

The boundary condition at the leading edge requires a stagnation point at the origin in the ζ-plane; this gives the condition

$$\frac{2\pi U\alpha}{\gamma} = \frac{1}{\zeta_o} + \frac{1}{\overline{\zeta}_o}$$

The condition imposed on the vortex system in the z-plane is that the net forces on the line vortex and the vortex sheet be zero.

The force on the vortex sheet per unit length is $\rho U \frac{d\gamma}{ds} (z_o - a + ia \cot \beta\pi)$.* The force on the line vortex per unit length is $-\rho v^* \gamma$, where v^* is the velocity normal to the vortex.

Therefore, equating the two vector forces

---

* Cosines of small angles are taken equal to unity; sines of small angles are taken equal to the angle.

$$v^* = \frac{U}{\gamma} \frac{d\gamma}{ds} (z_o - a + ia \cot \beta\pi)$$

Now

$$\epsilon = \frac{a}{s} \quad , \quad \gamma = s \frac{d\gamma}{ds}$$

$$v^* = \frac{U\epsilon}{a} (z_o - a + ia \cot \beta\pi)$$

The velocity v^* consists of two components, one due to the component of the free stream normal to the vortex and the other due to the disturbance potential.

$$v^* = U^* + (u + iv)_{z_o}$$

where $(u + iv)_{z_o}$ is the mean value as $z \rightarrow z_o$.

$$U^* = - U\epsilon \frac{(z_o + ia \cot \beta\pi)}{a}$$

$$v^* = -U\epsilon \frac{(z_o + ia \cot \beta\pi)}{a} + (u + iv)_{z_o}$$

The mean complex velocity at the vortex position is obtained by considering the complex potential function from which the complex potential function due to the vortex at z_o has been subtracted. We define

$$F_1 = F + \frac{i\gamma}{2\pi} \ell n (z - z_o)$$

then

$$\frac{dF_1}{dz} = u - iv$$

$$v^* = -U\epsilon \frac{(z_o + ia \cot \beta\pi)}{a} + \overline{(\frac{dF_1}{dz})_{z_o}}$$

$$= U\epsilon \frac{(z_o - a + ia \cot \beta\pi)}{a}$$

Therefore, finally we obtain

$$\overline{(\frac{dF_1}{dz})_{z_o}} = U\epsilon [\frac{2z_o}{a} + 2i \cot \beta\pi - 1]$$

or

$$(W_1)_{z_o} = (\frac{dF_1}{dz})_{z_o} = U\epsilon [\frac{2\overline{z}_o}{a} - 2i \cot \beta\pi - 1]$$

We now substitute F_1 into this equation to obtain our equation, the solution of which will yield z_o.

$$F_1 = -\frac{i\gamma}{2\pi} [\ell n (\zeta - \zeta_o) - \ell n (\zeta + \overline{\zeta}_o) - \ell n (z - z_o)] - iU a\zeta$$

or

$$F_1 = [\frac{i\gamma}{2\pi} \ell n (\zeta + \overline{\zeta}_o) - iU a\zeta] - \frac{i\gamma}{2\pi} [\ell n(z - z_o) - \ell n (\zeta - \zeta_o)]$$

Now

$$W_1 = \frac{dF_1}{dz} = \frac{dF_1}{d\zeta} \Big/ \frac{dz}{d\zeta} = \frac{1}{f'} (\frac{i\gamma}{2\pi} \frac{1}{\zeta + \overline{\zeta}_o} - iU a) - \frac{i\gamma}{2\pi} (\frac{1/f'}{\zeta - \zeta_o} - \frac{1}{z - z_o})$$

Consider the singular part of W_1 as $\zeta \to \zeta_o$,

$$\left[\frac{1/f'}{\zeta-\zeta_o} - \frac{1}{z-z_o}\right]_{\zeta\to\zeta_o} = \left[\frac{(z-z_o)-f'(\zeta-\zeta_o)}{f'(\zeta-\zeta_o)(z-z_o)}\right]_{\zeta\to\zeta_o}$$

We expand z in a Taylor series

$$z = f(\zeta_o) + f'(\zeta_o)\,(\zeta-\zeta_o) + \tfrac{1}{2}f''_o(\zeta-\zeta_o)^2 + \ldots$$

$$z_o = f(\zeta_o)$$

$$z-z_o = f'(\zeta_o)(\zeta-\zeta_o) + \tfrac{1}{2}f''\,(\zeta_o)(\zeta-\zeta_o)^2$$

Substituting

$$\left[\frac{(z-z_o)-f'(\zeta-\zeta_o)}{f'(\zeta-\zeta_o)(z-z_o)}\right]_{\zeta\to\zeta_o} =$$

$$= \left[\frac{f'_o(\zeta-\zeta_o)+\frac{1}{2}f''_o(\zeta-\zeta_o)^2-f'_o(\zeta-\zeta_o)-f''_o(\zeta-\zeta_o)^2}{(\zeta-\zeta_o)[f'_o+f''_o\,(\zeta-\zeta_o)]\,[f'_o(\zeta-\zeta_o)+\frac{1}{2}f''_o\,(\zeta-\zeta_o)^2]}\right]_{\zeta\to\zeta_o} = -\tfrac{1}{2}\frac{f''_o}{(f'_o)^2}$$

Thus

$$(W_1)_{\zeta_o} = \left[\frac{1}{f'_o}\left(\frac{i\gamma}{2\pi}\frac{1}{\zeta+\overline{\zeta}_o} - iU\alpha\right)\right] + \frac{i\gamma}{4\pi}\frac{f'''_o}{(f'_o)^2}$$

and from the boundary condition at the leading edge

$$\frac{\gamma}{2\pi} = U\alpha\,\frac{\zeta_o\overline{\zeta}_o}{\zeta_o+\overline{\zeta}_o}$$

Substituting for γ in the above expression and substituting $(W_1)_{\zeta_o}$ into the vortex force balance equation, we get

$$\frac{ia}{f'_o}\left(\frac{\zeta_o\bar{\zeta}_o}{\zeta_o+\bar{\zeta}_o} - 1 + \tfrac{1}{2}\frac{f''_o}{f'_o}\right) = \epsilon\left(\frac{2z_o}{a} - 2i\cot\beta\pi - 1\right) - (1)$$

where for the triangular shape

$$f'(\zeta) = A\left(\frac{\zeta}{\zeta-i}\right)^{\beta}\left(\frac{\zeta}{\zeta+ic}\right)^{\frac{1}{2}}$$

and

$$f''(\zeta) = A\,\frac{\zeta^{\beta+\frac{1}{2}}}{(\zeta-i)^{\beta}(\zeta+ic)^{\frac{1}{2}}}\left[\frac{\beta+\frac{1}{2}}{\zeta} - \frac{\beta}{(\zeta-i)} - \tfrac{1}{2}\frac{1}{(\zeta+ic)}\right]$$

Equation 1 may be solved numerically for ζ_o. Unfortunately, the term on the right hand side involving $\bar{z}_o$ cannot be eliminated.

Therefore, the only method of solution is that of iteration. A value of z_o is assumed and substituted into the equation, which is then solved numerically for ζ_o. This description is, of course, purely formal; in the actual computation one has to work with both the real and imaginary components of ζ and z.

Once a value for ζ_o is obtained, the corresponding value of z_o is found and compared to the assumed value. If the two do not agree, the computed value of z_o is substituted back into the equation and the procedure repeated until the desired accuracy is obtained.

As can be seen by looking at the expression for f' and f'', this computation would be extremely long and tedious.

The experimental results show that the mathematical model of two vortices does not properly represent the physical flow picture. Since it was not considered to have sufficient practical value here, the lengthy computation for the vortex position was not carried out.

III. DESCRIPTION OF MODELS AND TESTS

A. Wind-Tunnel Models

Four delta wings of identical planform but with triangular cross section of varying thickness were tested in the 10-ft. GALCIT wind tunnel. The proportions and dimensions of these models are shown in Fig. 3.

The seminose angle ϵ for all models was 15° and the length 48".

Model A: Flat aluminum plate with fin on lower side for structural rigidity. 26 pressure orifices on both top and bottom surfaces. Leading edges bevelled at 45°.

Models B, C, D: Wooden models with milled aluminum leading edges. Triangular cross section with included angle at leading edge of 10, 20, 30°, respectively.

The models were stingmounted and the sting was attached to a heavy U-shaped tube pivoting at the side walls of the tunnel about a line through the center of lift of the model.

The models each have pressure orifices at three stations along the wing at 40, 70, and 97 per cent of wing length. Additional orifices are located on the base.

No direct lift or drag measurements were made.

B. Test Conditions

Pressure data were recorded photographically for each of

the four models for angles of attack between -2° and 20° and at 2° intervals. These measurements were repeated for several values of q between 15 psi and 50 psi to ascertain that there was no dependence on Reynolds number.

Tufts were attached on the models and photographs taken to study the air flow over the top and bottom surfaces of the wings.

IV. RESULTS AND CONCLUSIONS

A. Spanwise Pressure Distribution

The results are plotted in Figs. 6 - 25. Figs. 6 - 19 show the spanwise pressure distributions for the different wings and at the various stations. The distribution for the lower surface is given only for model A. Since only a few pressure orifices were located on the lower surface of the other three models, only the average pressure on that surface is given in tables adjoining Figs. 8 - 10.

It is evident upon inspection of Figs. 6 - 14 that there exist one or more small vortices besides the main one; these are seen to be very near the leading edge. Unfortunately, the spacing of pressure orifices on the present models was not close enough to definitely determine the pressure distribution in the region $.9 < x^* \leq 1.0$.

It should be possible in future research to study the flow field in the immediate neighborhood of the leading edge by means of small, closely-spaced, pressure orifices and by flow visualization techniques. It may turn out to be possible to influence the main flow field above the wing by manipulation of the flow near the leading edge and to produce favorable results such as an increase in lift.

Figs. 6 and 7 show the pressure distributions for the upper and lower surfaces of model A. The effect of the small leading-edge vortices is clearly visible. It is probable that the pressure for small angles of attack is influenced to a certain degree by the finite thickness of the plate; however, this effect will be less serious for larger values of α.

Similar distributions for models B, C, D are shown in Figs. 8 - 10. The lift decrease with increasing θ can be clearly seen.

The pressure distributions at station 3 near the trailing edge for the four models are plotted in Figs. 11 - 14. The effect of θ at this station is almost nonexistent. The curves of C_p at any constant value of α are practically identical for the four values of θ: they differ possibly near the leading edge.

Figs. 15 - 18 show the pressure variation along the wing by means of plots for stations 1, 2, and 3 at a few angles of attack. It is seen that the flow field is very nearly conical over a large part of the wing at small angles of attack. But at large angles of attack, the departure from conical flow becomes marked.

Fig. 19 shows the effect of θ on the pressure distribution at a constant angle of attack of 12°. The distribution predicted by the Brown and Michael theory for the flat wing is also shown for comparison. One interesting fact is that although the experimental and theoretical distributions differ strongly, their integrals over the span agree very closely, as is shown later in Fig. 22.

B. Vortex Position

The position of the peak of the negative pressure plot on the upper surface may be taken as the approximate position of the vortex above that surface. This distance, designated as $(\frac{x}{a})_{min} C_p$, is shown plotted versus α in Fig. 20, and versus the local lift coefficient C_ℓ in Fig. 21. The curve predicted by the Brown and Michael theory is also shown.

As θ increases, the vortex at first moves towards the center, but then this trend reverses and the vortex begins to move away from the center. The reason for this is not clear.

C. Local Lift and Drag Coefficients

The local spanwise lift coefficient is defined as

$$C_\ell = \int_0^1 (C_{p_{lower}} - C_{p_{upper}}) \, dx^* \cos \alpha$$

This coefficient is plotted versus α in Fig. 22. It is seen that the result for the flat wing agrees very closely with the results of Brown and Michael. The decline of lift with increasing θ at constant α has been noted before.

If we now make a simple geometrical definition for a corrected angle of attack

$$\alpha^* = \alpha - \frac{\sigma}{2} \qquad \text{where} \qquad \sigma = \tan^{-1} [\tan \epsilon \tan \theta]$$

then the value of C_ℓ versus α^* for all four models fall on a single curve with little scatter, as shown in Fig. 23.

The local drag coefficient for a flat wing is defined in analogy with C_ℓ as

$$C_{d_i} = \int_0^1 (C_{p_\ell} - C_{p_u}) \, dx^* \sin \alpha$$

For the wings with triangular cross section, the lift coefficient is less than that for the flat plate for a fixed value of α, and therefore the drag coefficient as a function of C_ℓ will be higher. But the lift vector is also tilted forward due to the forward-facing top surface,

and this in turn reduces the drag coefficient.

This drag-reducing component is

$$C_{d_{red}} = \int_0^1 C_{p_u} \, dx^* \tan\theta \sin\epsilon \cos\alpha$$

Taking this into account one obtains the true local drag coefficient, which is shown as a function of C_l in Fig. 24 for all four models. Note that the local drag coefficient is unaffected by θ, since the results for all wings fall on one curve.

In addition, there is, of course, the base drag which must be taken into account. This is plotted in Fig. 25. The conclusion is thus that a conical wing of purely triangular cross section has higher drag than a flat wing of the same planform and producing the same lift.

D. Reduction of Lift-Dependent Drag

G. H. Lee (Ref. 3) in 1959 conducted wind-tunnel tests on slender delta wings of a cross sectional shape designed to make use of the peculiar spanwise pressure distribution for reducing the lift-dependent drag below that of a flat or thin symmetrical wing. The cross section employed is shown in Fig. 4.

The wings he used were not conical all the way to the trailing edge, but were faired off from 0.7 chord to the trailing edge. Lee found substantial reduction of lift-dependent drag, up to 30 per cent, but realized that the effect of the rounded-off back end was not clear and certainly contributed to the drag reduction.

The experimental results obtained in this study may be applied to predict the qualitative behavior of drag as a function of θ, the angle of the step in Lee's model. Since the included angle at the leading edge is zero, it may be assumed that the pressure distribution for the flat wing can be applied directly in this case. This will certainly be a good approximation for small values of θ.

For purposes of this calculation, conical flow will be assumed, i.e., the local lift and drag coefficients at station 1 (40 per cent chord) will be used as lift and drag coefficients for the entire wing. Base drag coefficients are determined from base pressures measured for the corresponding triangular wings.

The drag-reducing component of the integrated pressure-force vector for the upper surface gives

$$C_{D_{red}} = \int_{\lambda}^{\mu} C_{p_u} dx^* \tan\theta \, \mu \sin\epsilon \cos\alpha$$

The base drag coefficient is

$$C_{D_{base}} = C_{p_{base}} (\mu^2 - \lambda^2) \tan\theta \tan\epsilon \cos\alpha$$

Thus, the net reduction of the drag coefficient is

$$\left[\int_{\lambda}^{\mu} C_{p_u} dx^* \, \mu \sin\epsilon - C_{p\,base} (\mu^2 - \lambda^2) \tan\epsilon \right] \cos\alpha \tan\theta$$

This shows that the quantity in brackets should be maximized by the proper choice of μ and λ. From Fig. 6 it can be seen that these should lie roughly in the intervals: $.8 < \mu < .9$, and $.5 < \lambda < .6$.

The above expression shows that the reduction in drag is

greatest for large θ. This statement is qualified by the limitation that for large θ the flow field will be altered appreciably.

Calculations were carried out for the following values of the variables involved: $\lambda = .5$, $\mu = .8$, $0 < \theta < 45°$. The results are plotted in Fig. 26. It is interesting to note that the drag reduction as a percentage of the flat-plate drag as computed here has a maximum value between $\alpha = 16°$ and $18°$. The drag reduction is about one tenth of the flat-plate drag for $\theta = 45°$ and $14 < \alpha < 22°$. For α below about $11°$, the thick wing has higher drag than the flat one.

For reasonably large θ, say near $45°$, the flow will be appreciably altered due to the sharp corners of the cross section. A cross section such as the one shown in Fig. 5 may be more successful for maintaining high lift in that case.

REFERENCES

1. Brown, C. E. and Michael, W. H.; The Effect of Leading Edge Separation on the Lift of a Delta Wing. Journal of the Aeronautical Sciences, 1954, Vol. 21, p. 690.

2. Lee, G. H.; Note on the Flow around Delta Wings with Sharp Leading Edges. Reports and Memoranda No. 3070, 1955.

3. Lee, G. H.; Reduction of Lift-Dependent Drag with Separated Flow. ARC C.P. No. 593, 1959.

4. Prandtl, L.; General Considerations on Flows of Compressible Fluids. NACA TM 805, 1936.

5. Spreiter, J. R.; Aerodynamic Properties of Slender Wing-Body Combinations at Subsonic, Transonic and Supersonic Speeds. NACA TN 1662, 1948.

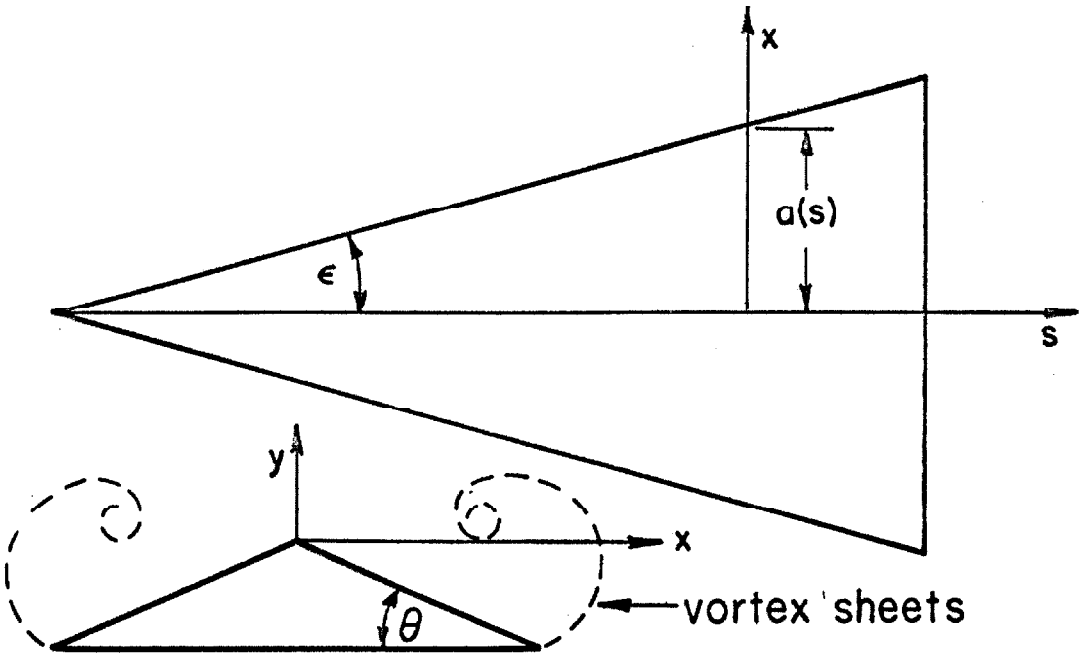

FIGURE 1

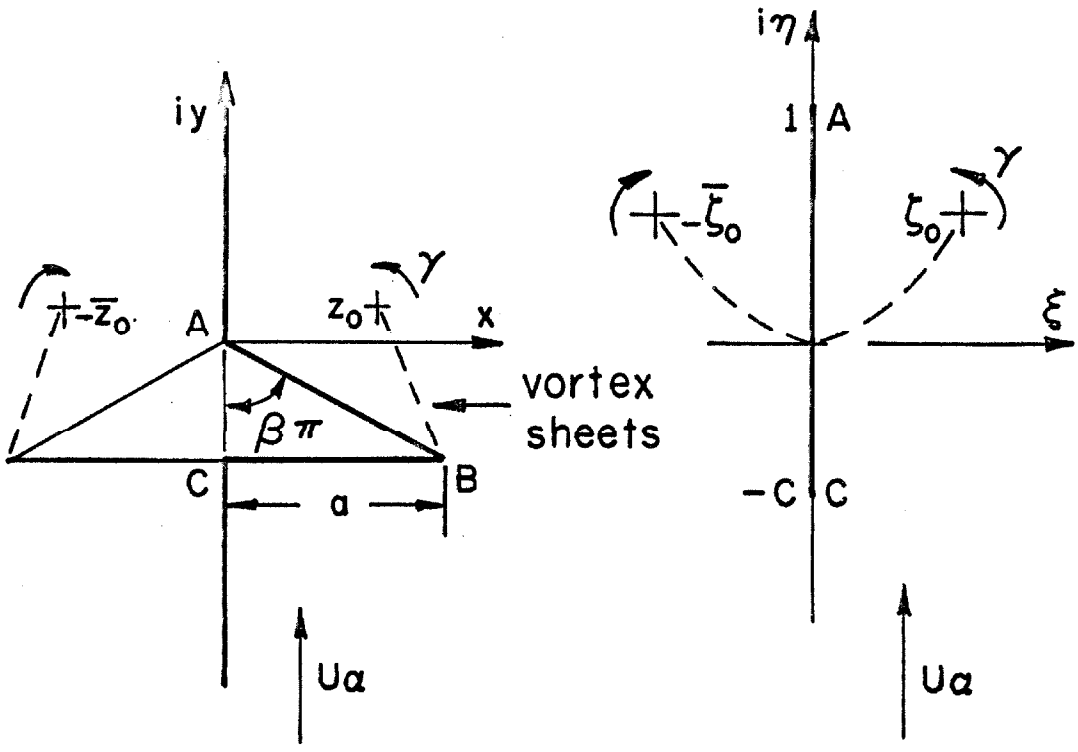

FIGURE 2

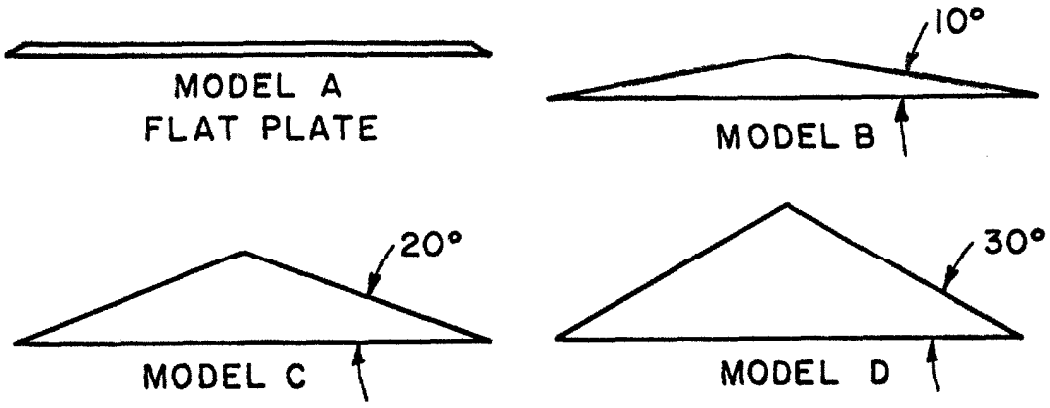
MODEL A
FLAT PLATE
10°
MODEL B
20°
MODEL C
30°
MODEL D

FIGURE 3

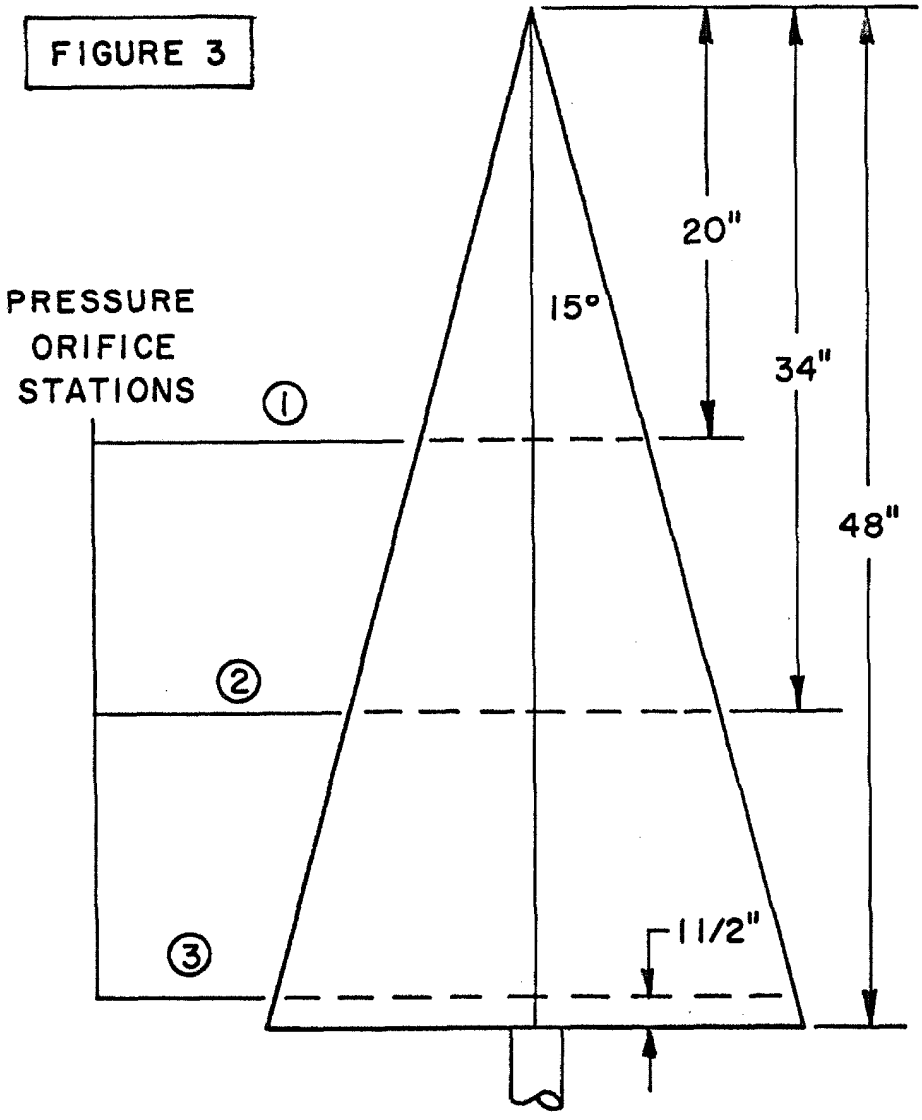
PRESSURE
ORIFICE
STATIONS
①
②
③
15°
20"
34"
48"
1 1/2"

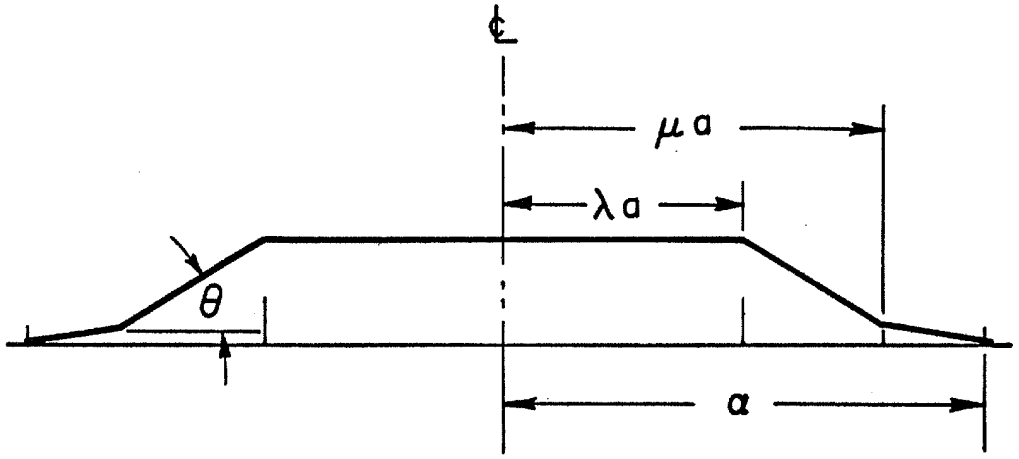

FIGURE 4

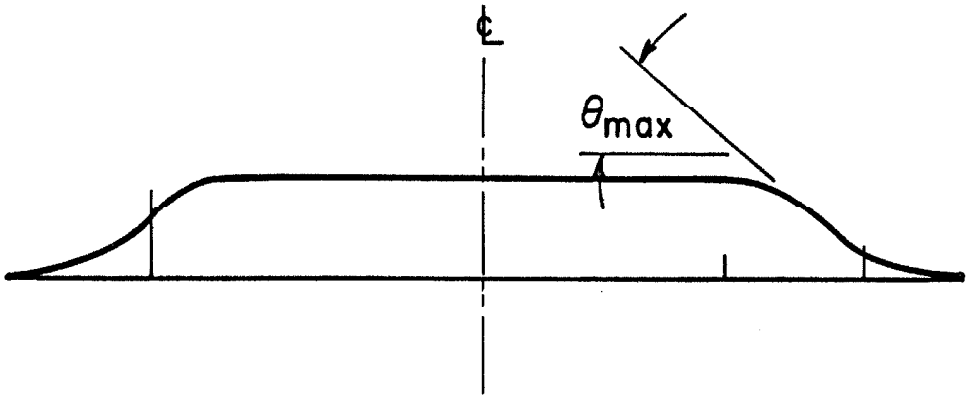

FIGURE 5

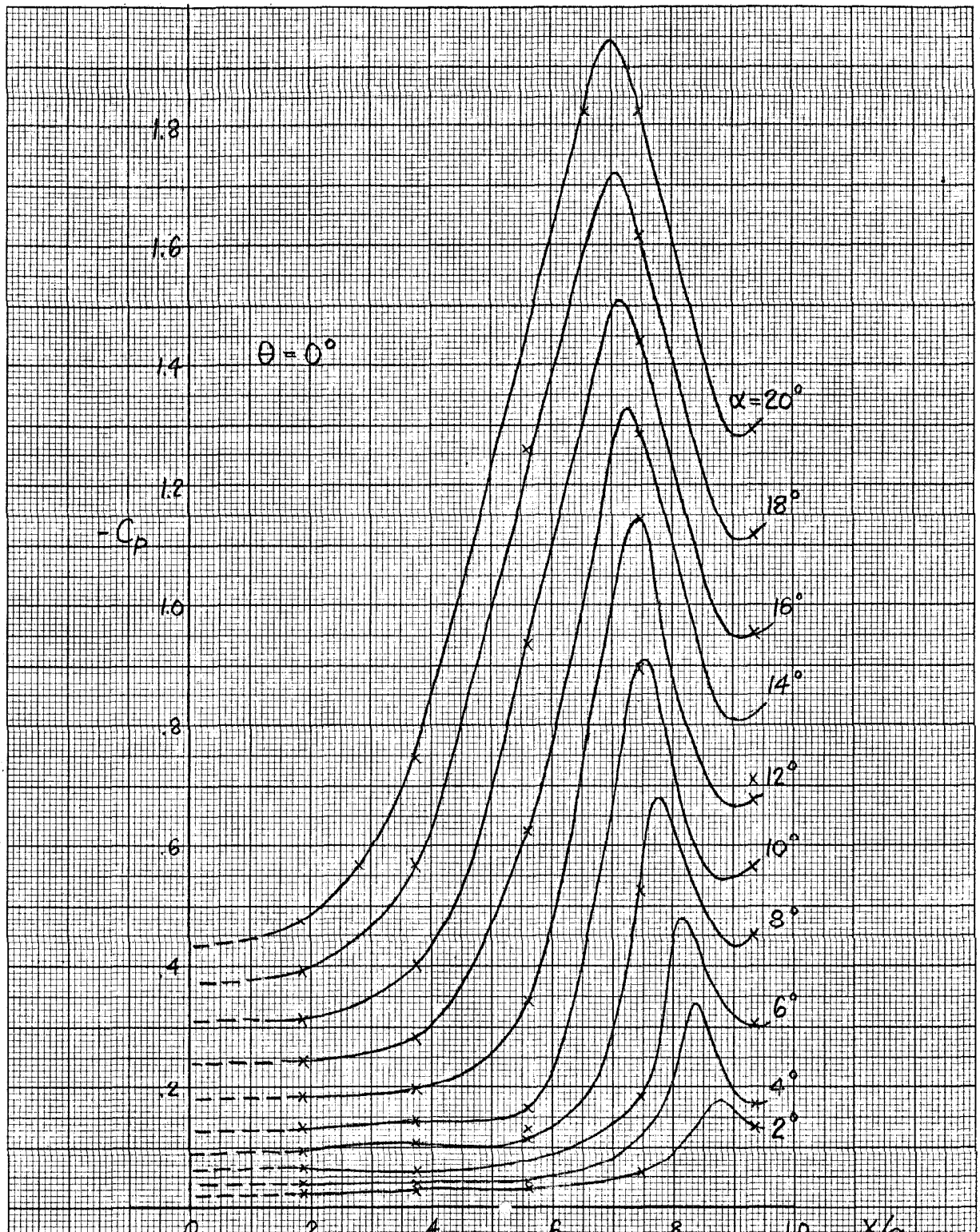

FIGURE 6: C_p DISTRIBUTION FOR MODEL A AT STATION 1.

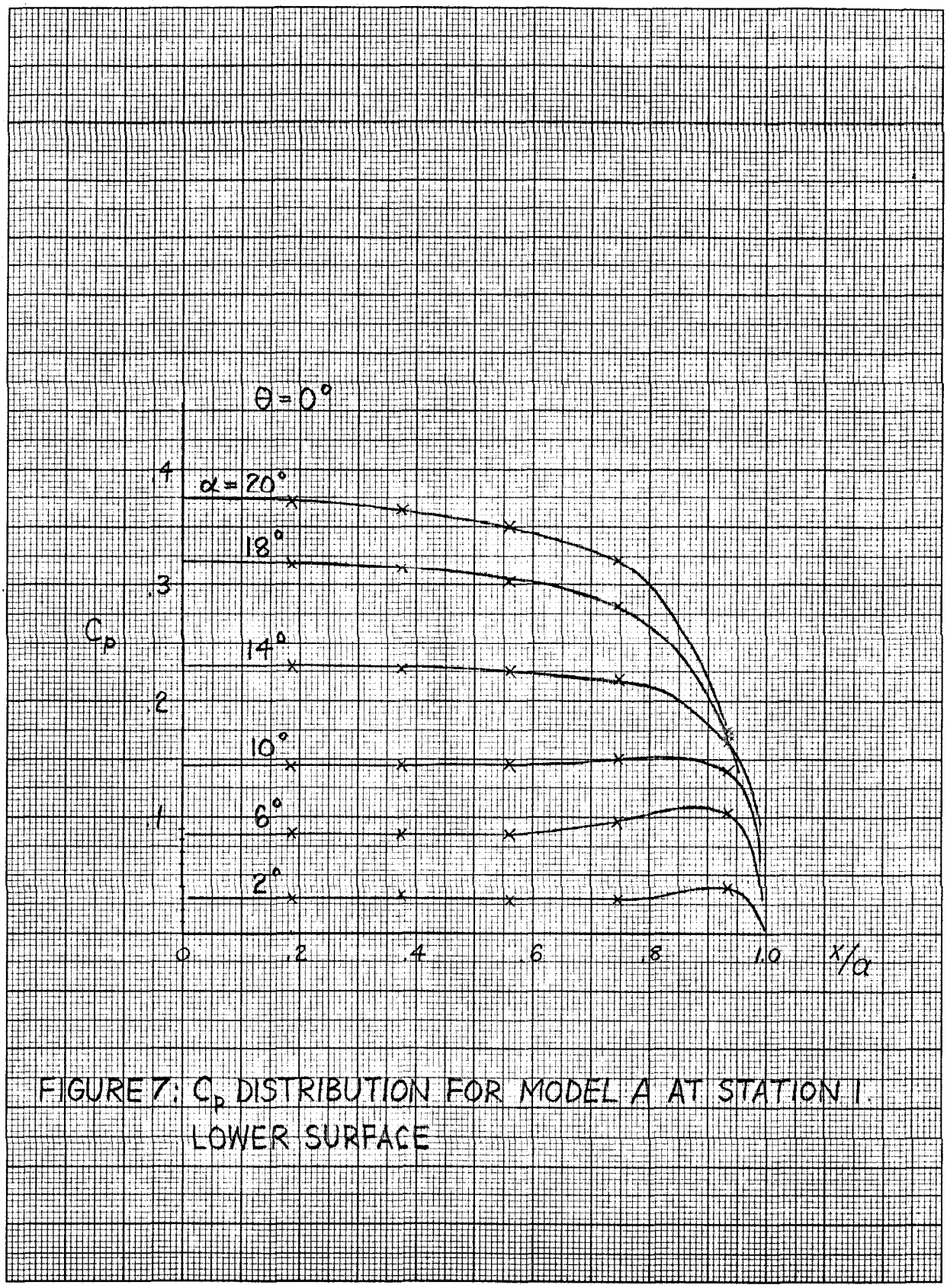

FIGURE 7: C_p DISTRIBUTION FOR MODEL A AT STATION 1. LOWER SURFACE

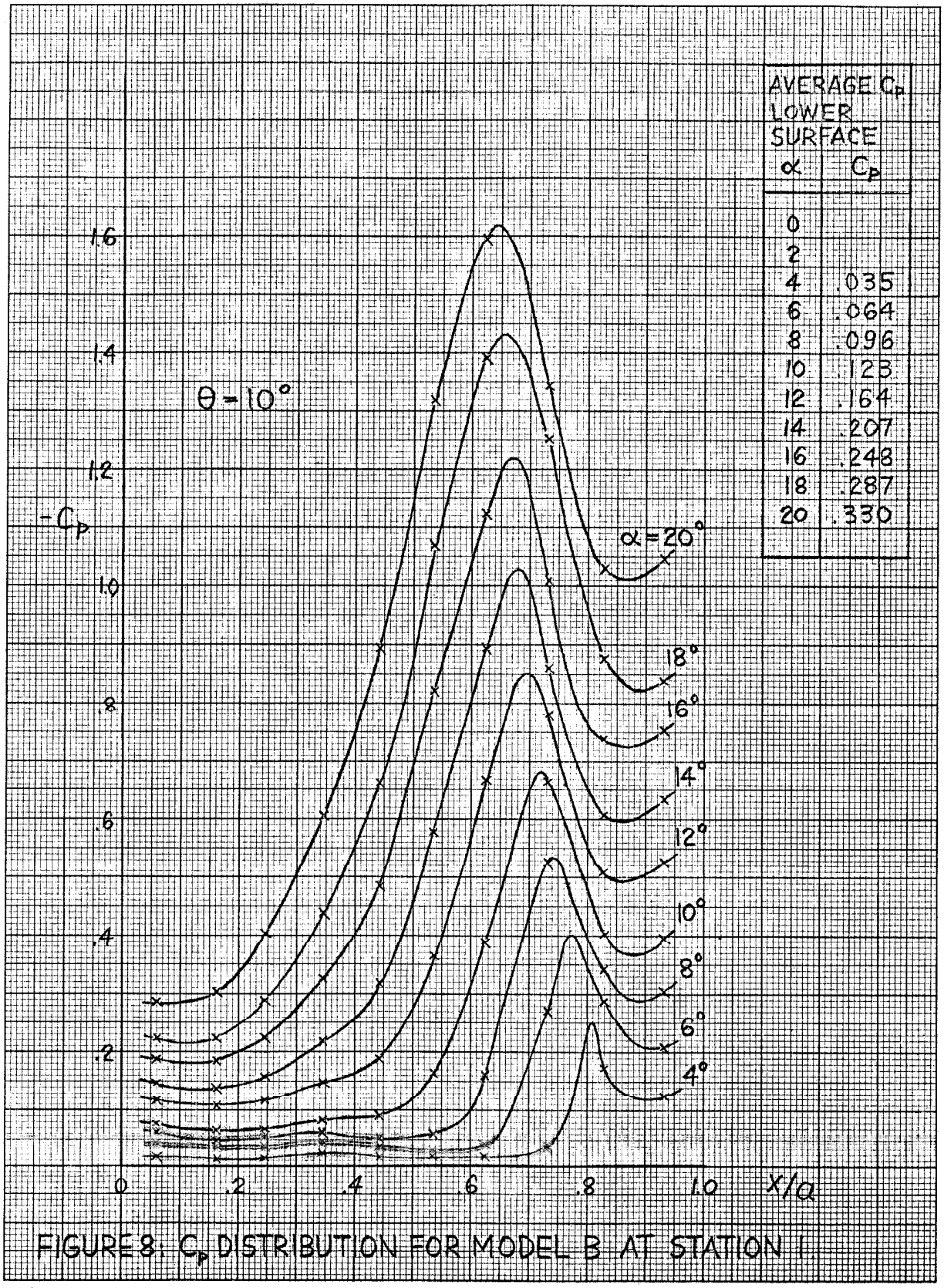

FIGURE 8: C_p DISTRIBUTION FOR MODEL B AT STATION 1

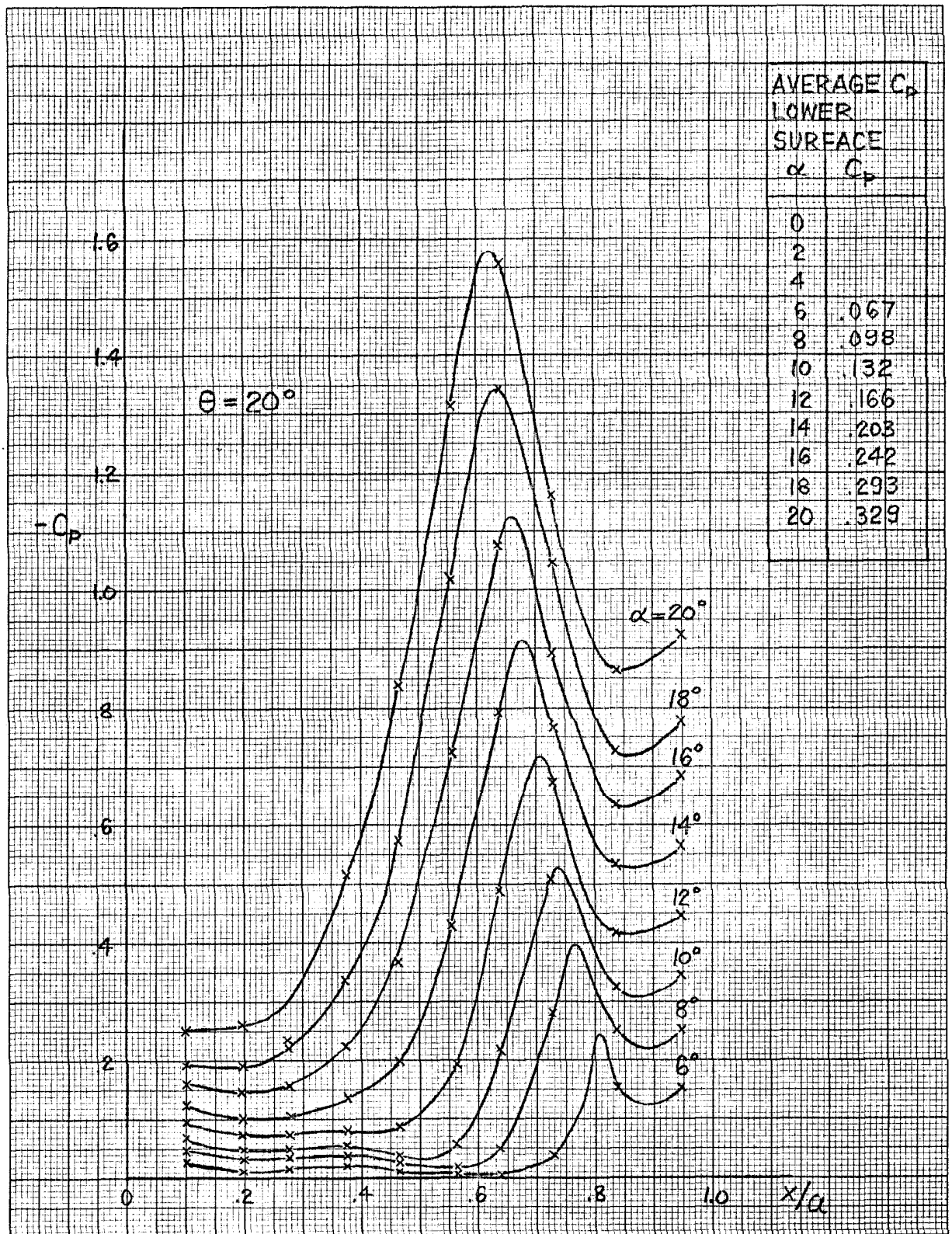

FIGURE 9: C_p DISTRIBUTION FOR MODEL C AT STATION 1.

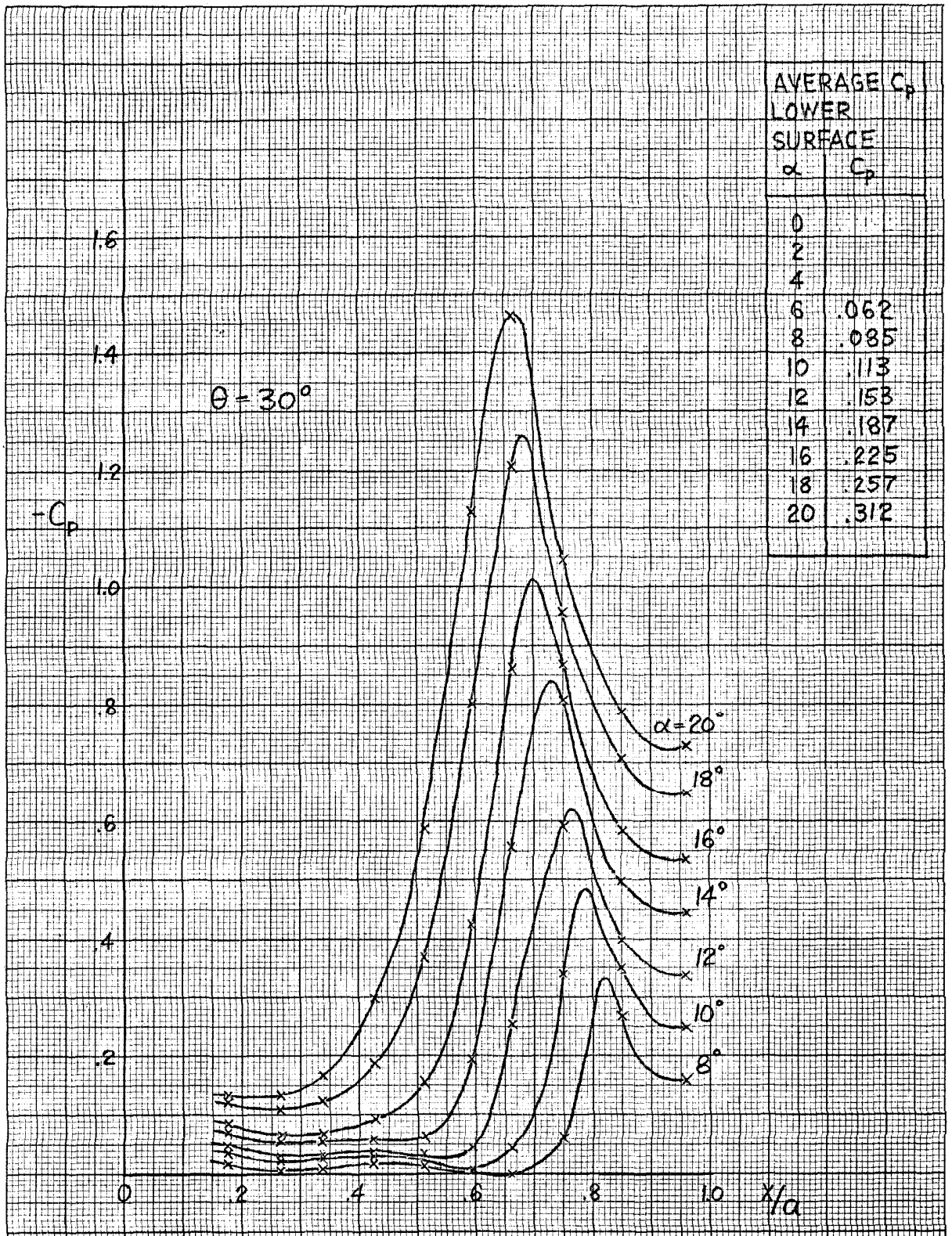

FIGURE 10: C_p DISTRIBUTION FOR MODEL D AT STATION 1.

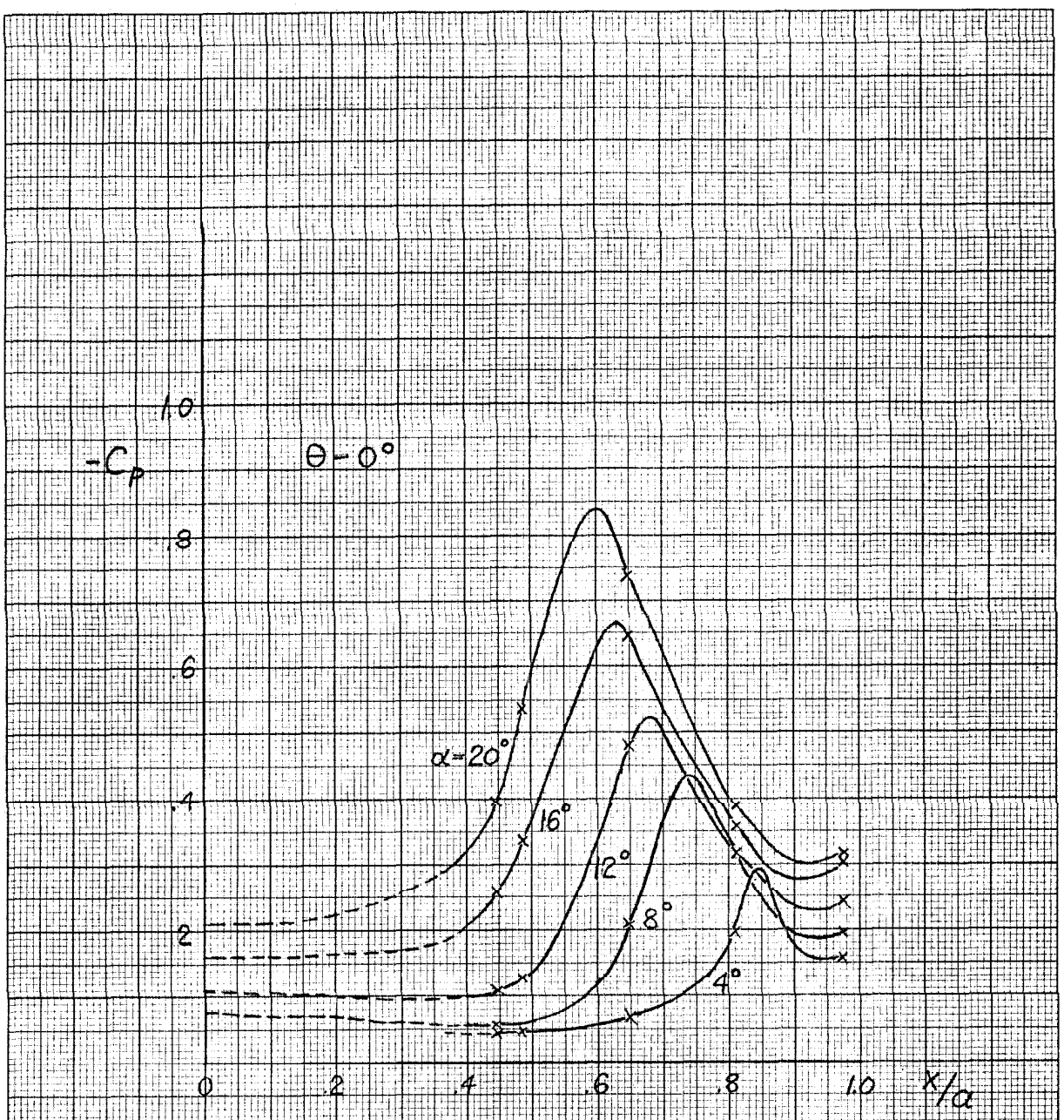

FIGURE 11: C_p DISTRIBUTION FOR MODEL A AT STATION 3

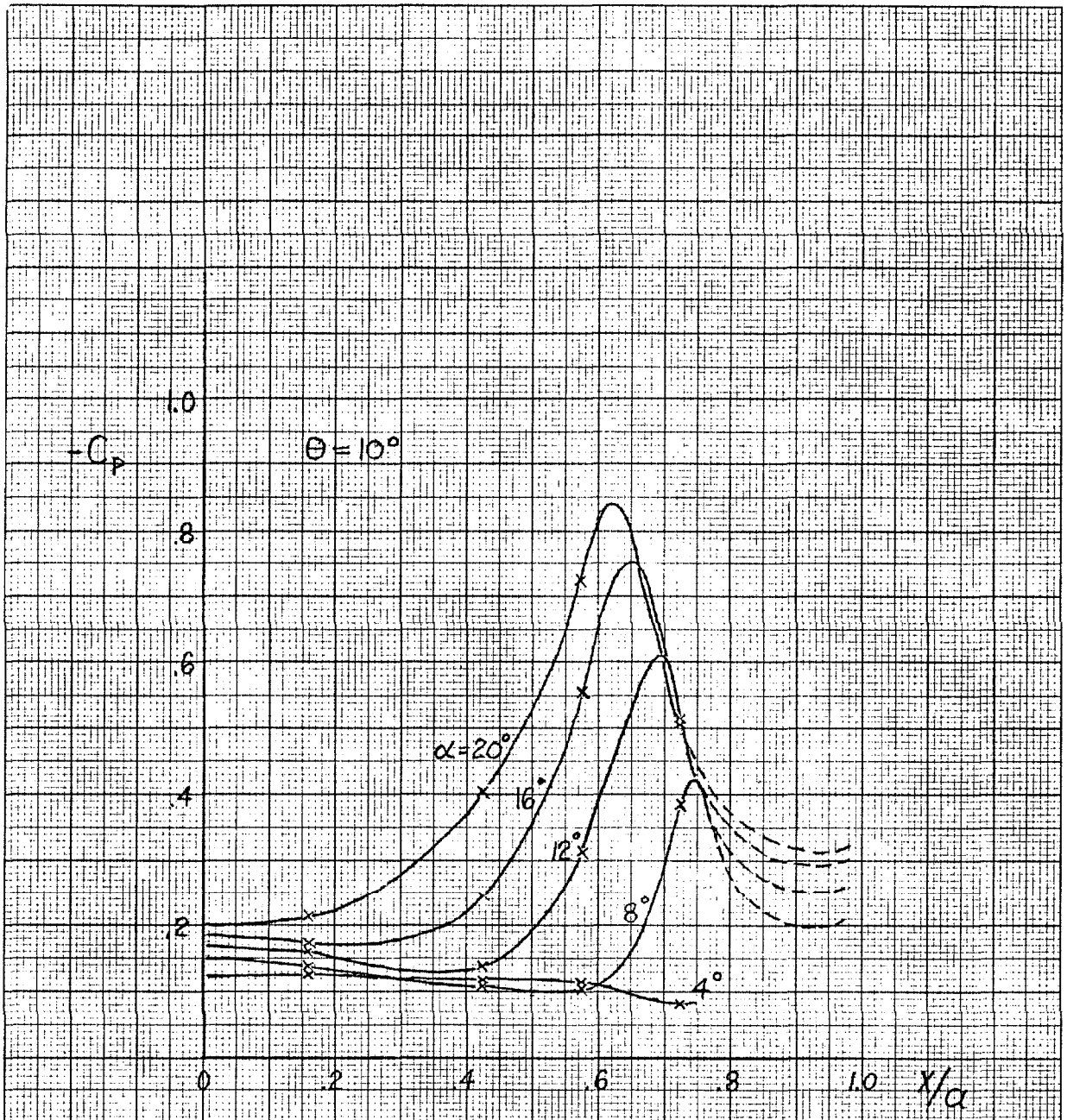

FIGURE 12. C_p DISTRIBUTION FOR MODEL B AT STATION 3.

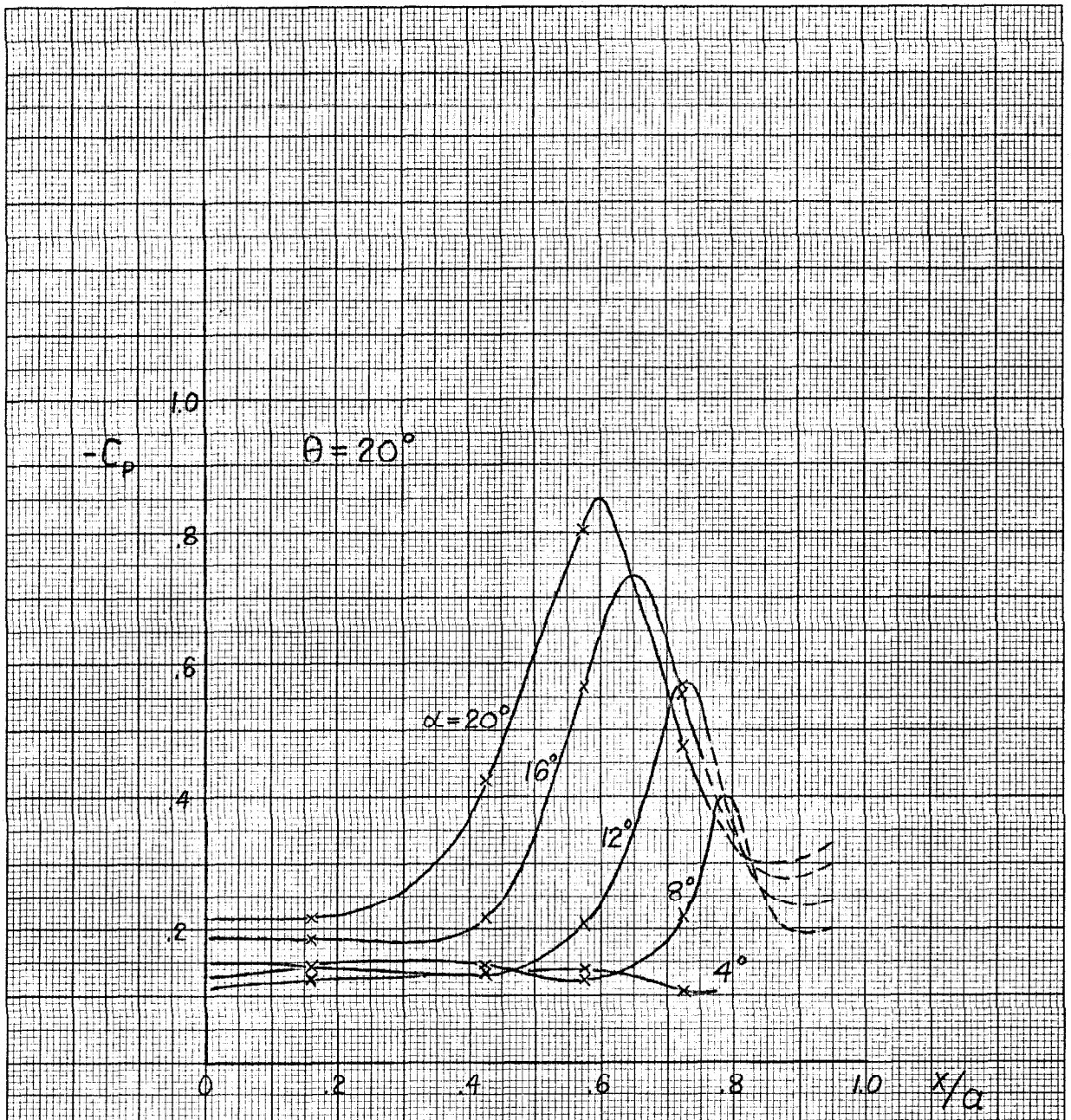

FIGURE 13: C_p DISTRIBUTION FOR MODEL C AT STATION 3.

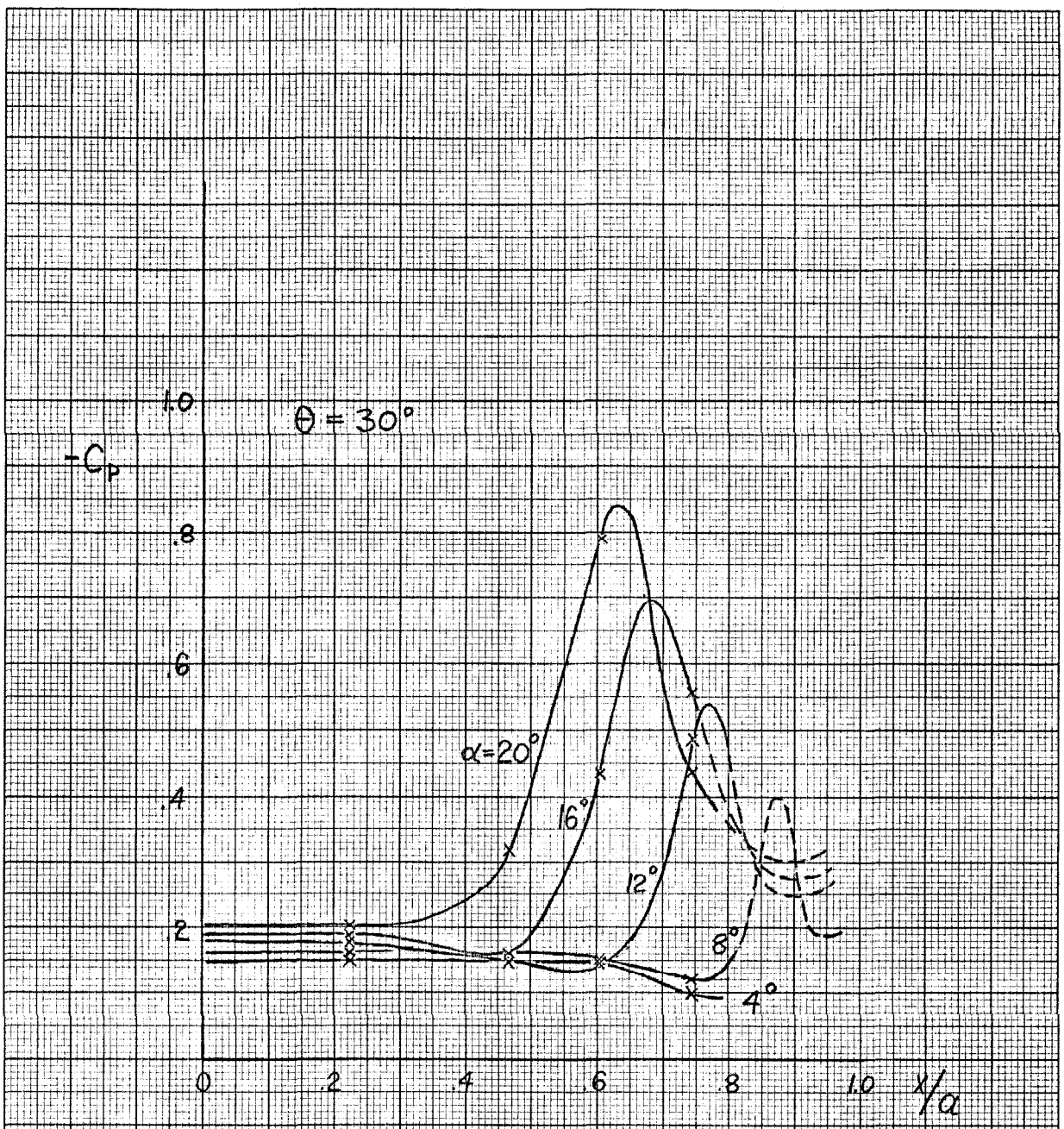

FIGURE 14: C_p DISTRIBUTION FOR MODEL D AT STATION 3

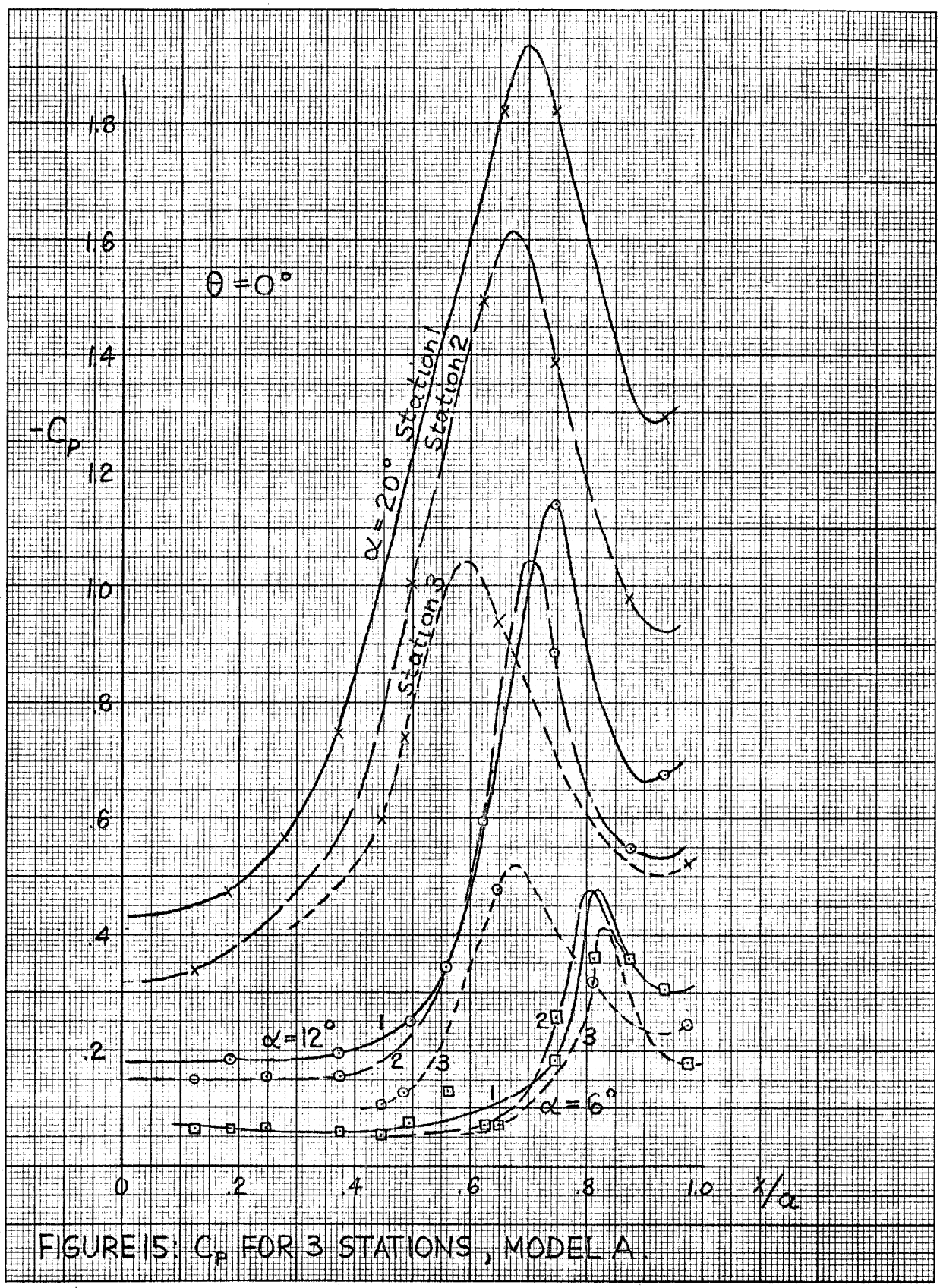

FIGURE 15: C_p FOR 3 STATIONS, MODEL A

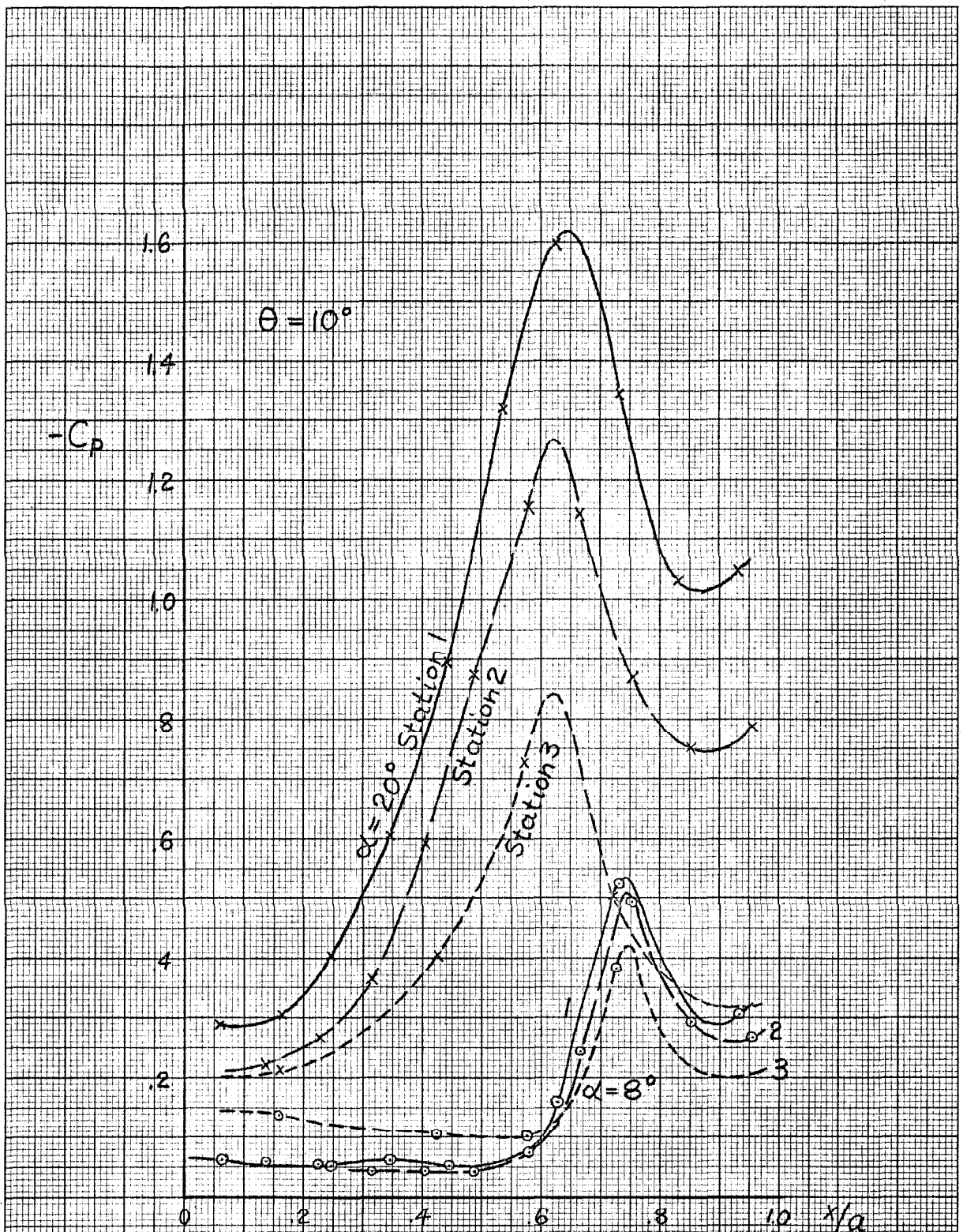

FIGURE 16: C_p FOR 3 STATIONS, MODEL B

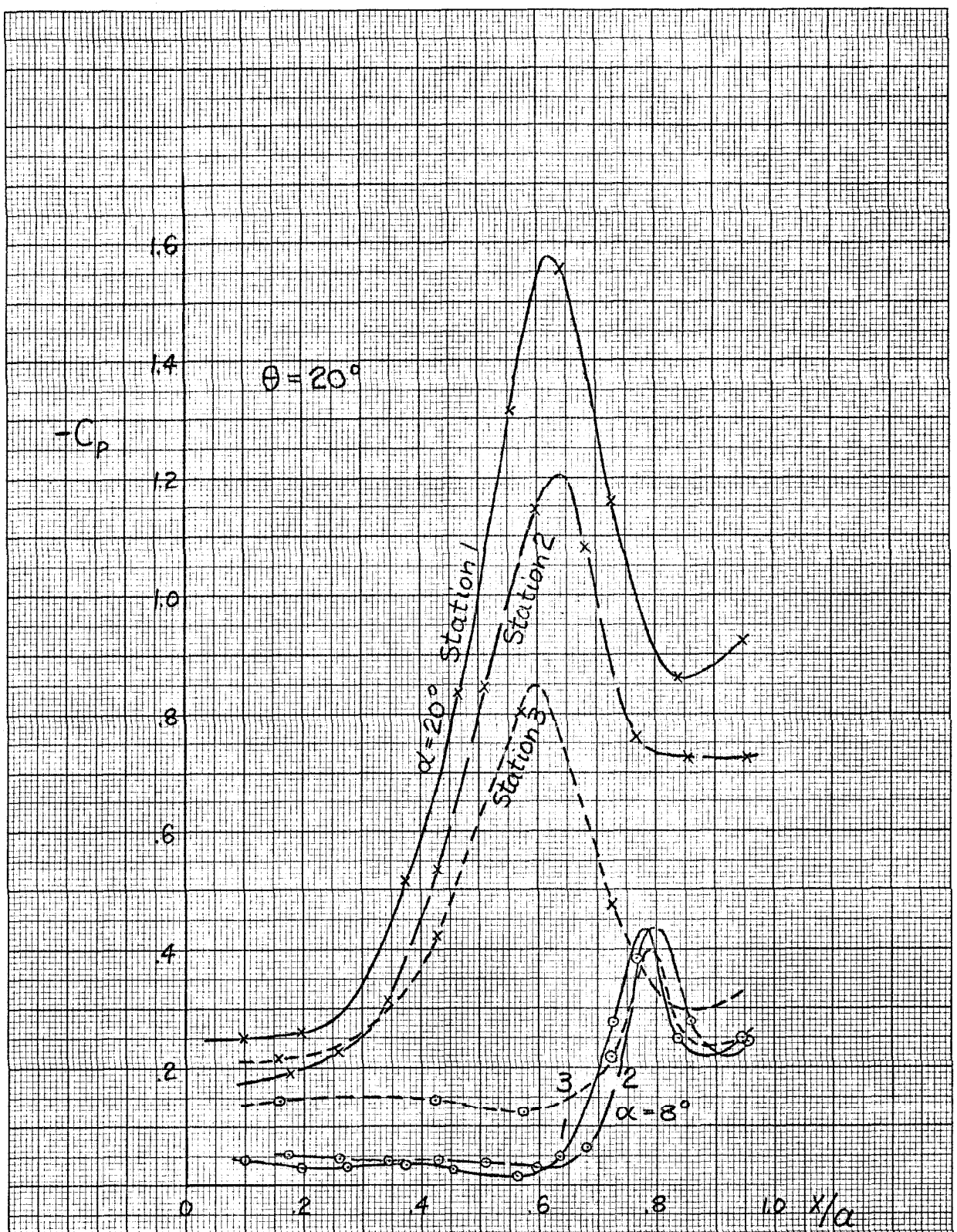

FIGURE 17: C_p FOR 3 STATIONS, MODEL C

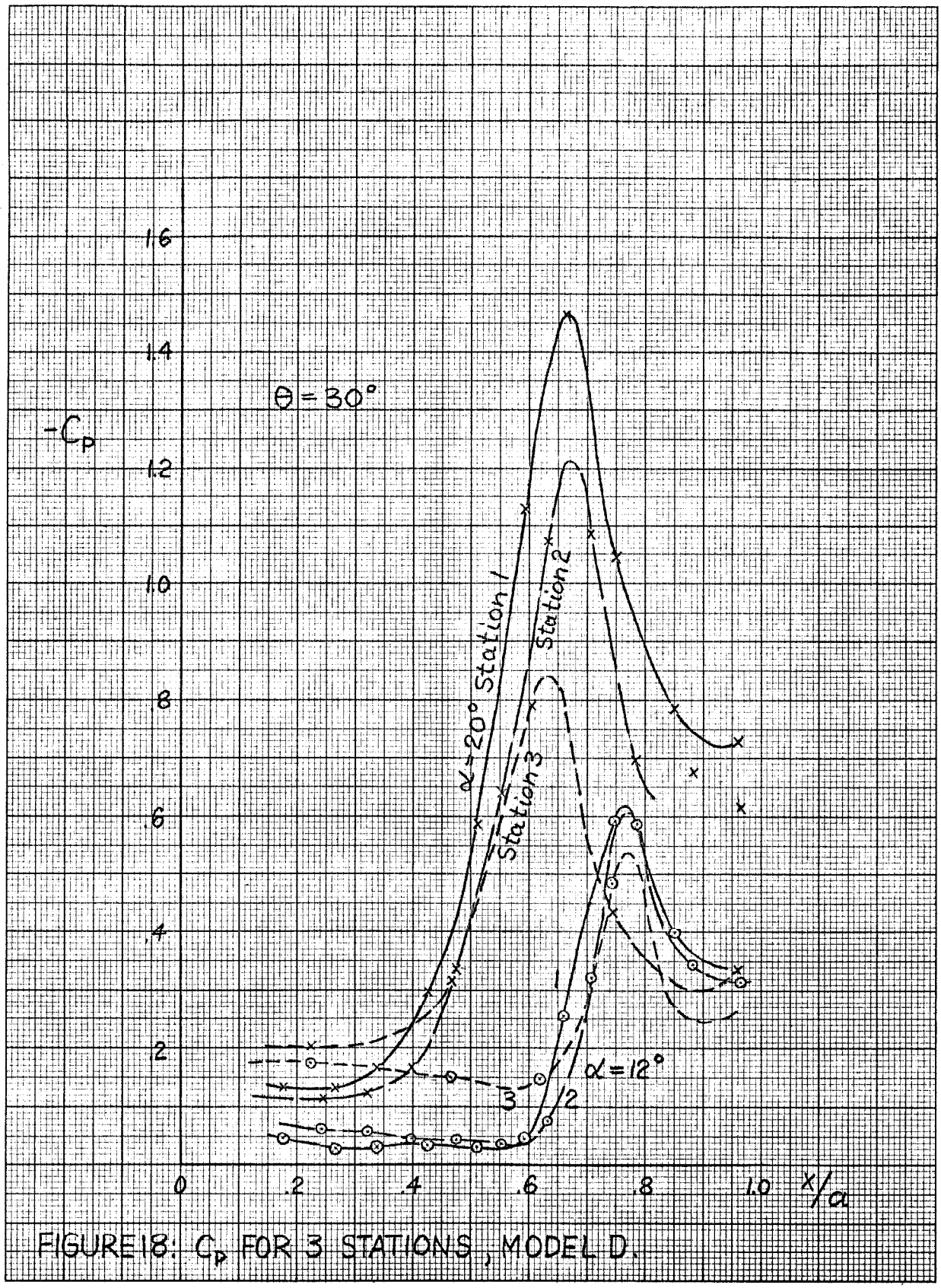

FIGURE 18: C_p FOR 3 STATIONS, MODEL D.

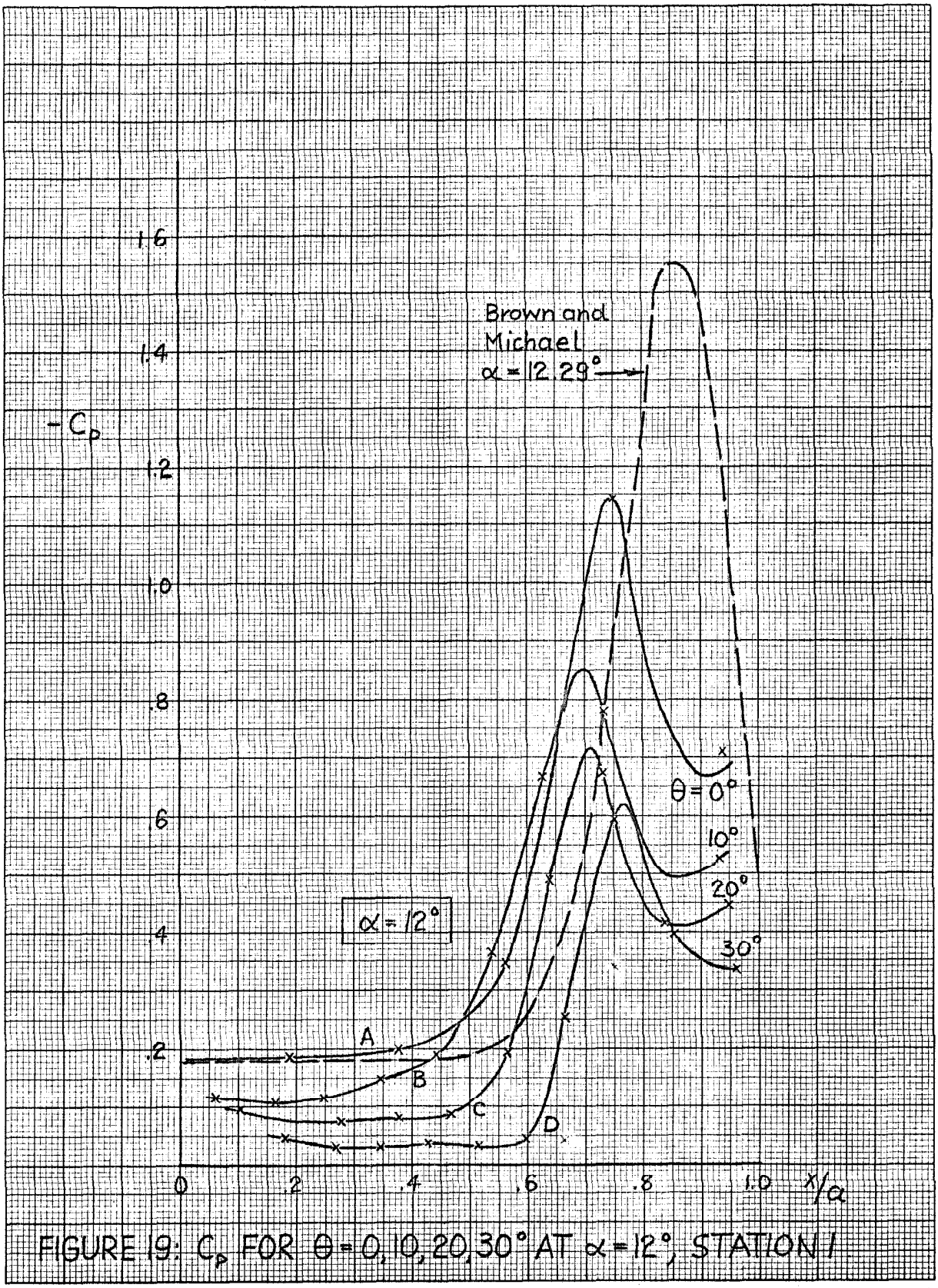

FIGURE 19: C_p FOR $\theta = 0, 10, 20, 30°$ AT $\alpha = 12°$, STATION I

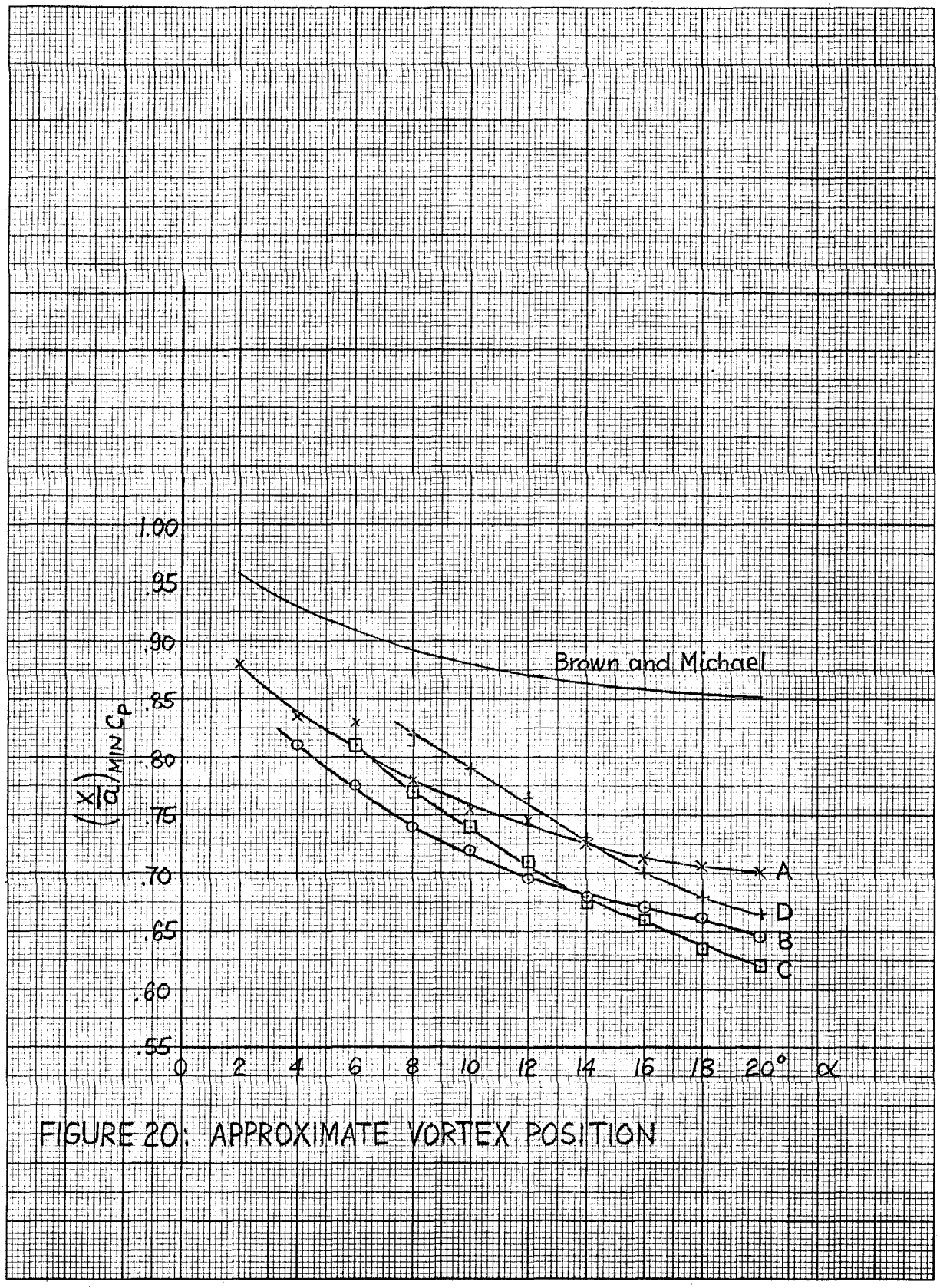

FIGURE 20: APPROXIMATE VORTEX POSITION

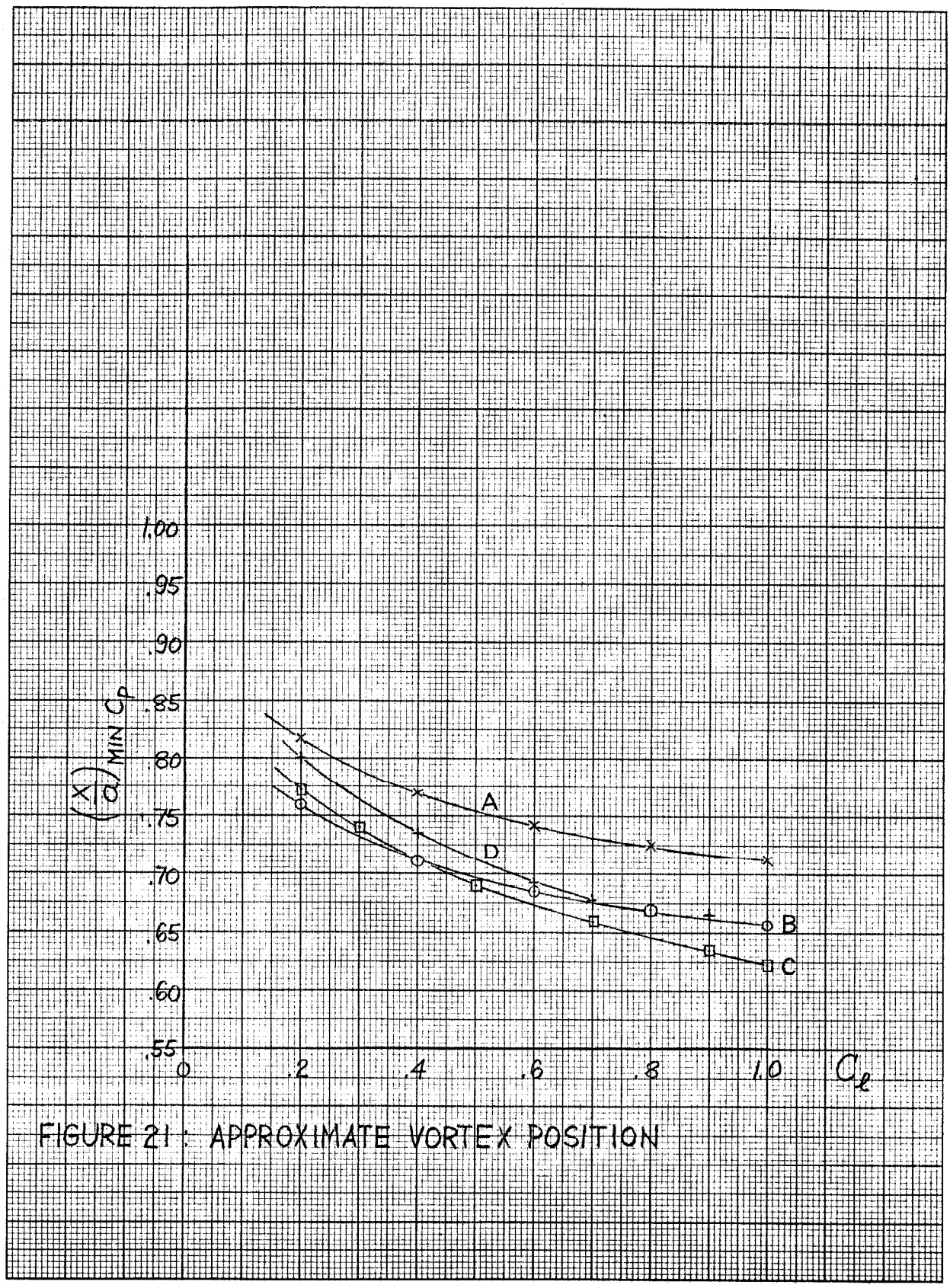

FIGURE 21: APPROXIMATE VORTEX POSITION

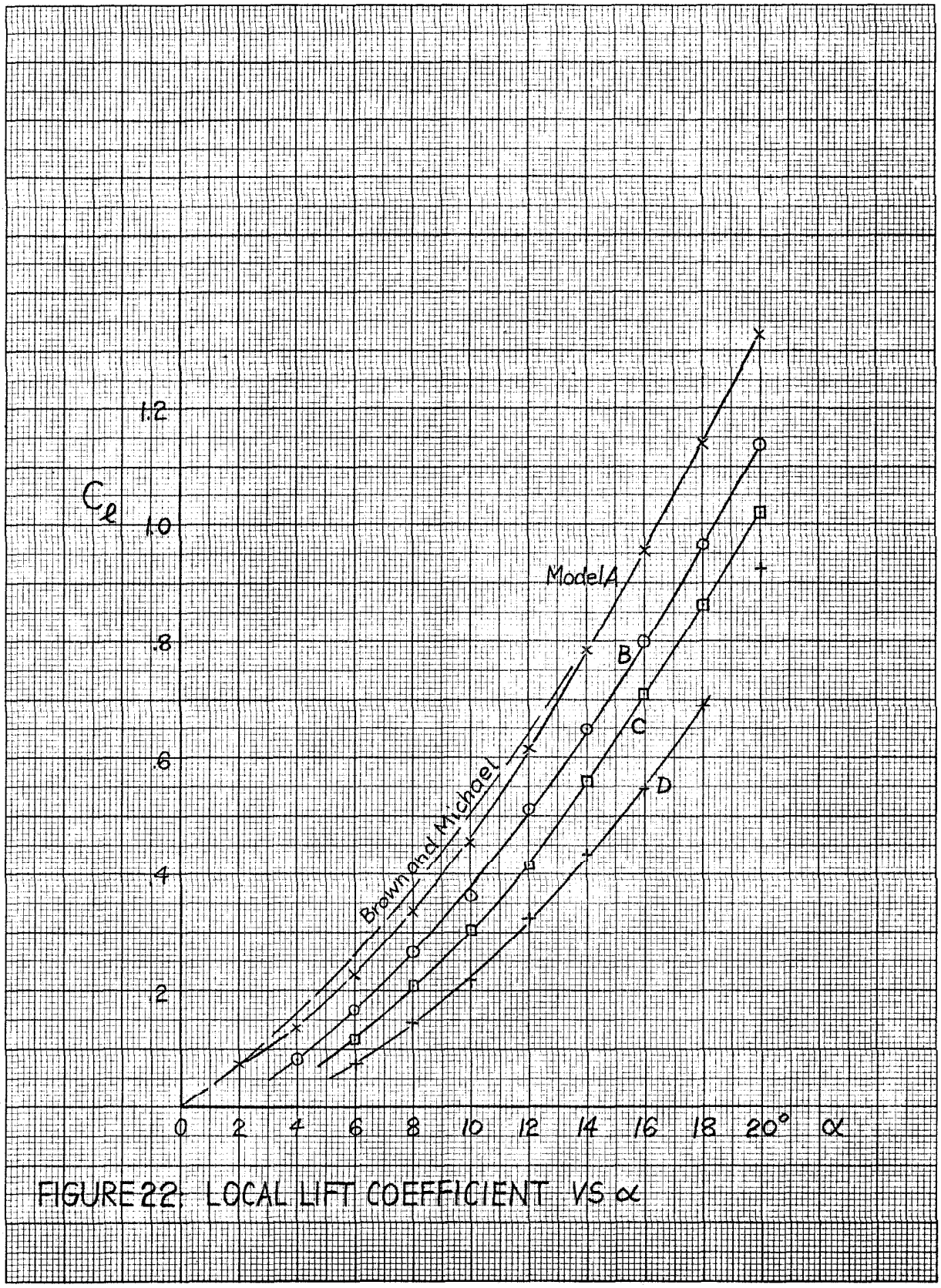

FIGURE 22: LOCAL LIFT COEFFICIENT VS α

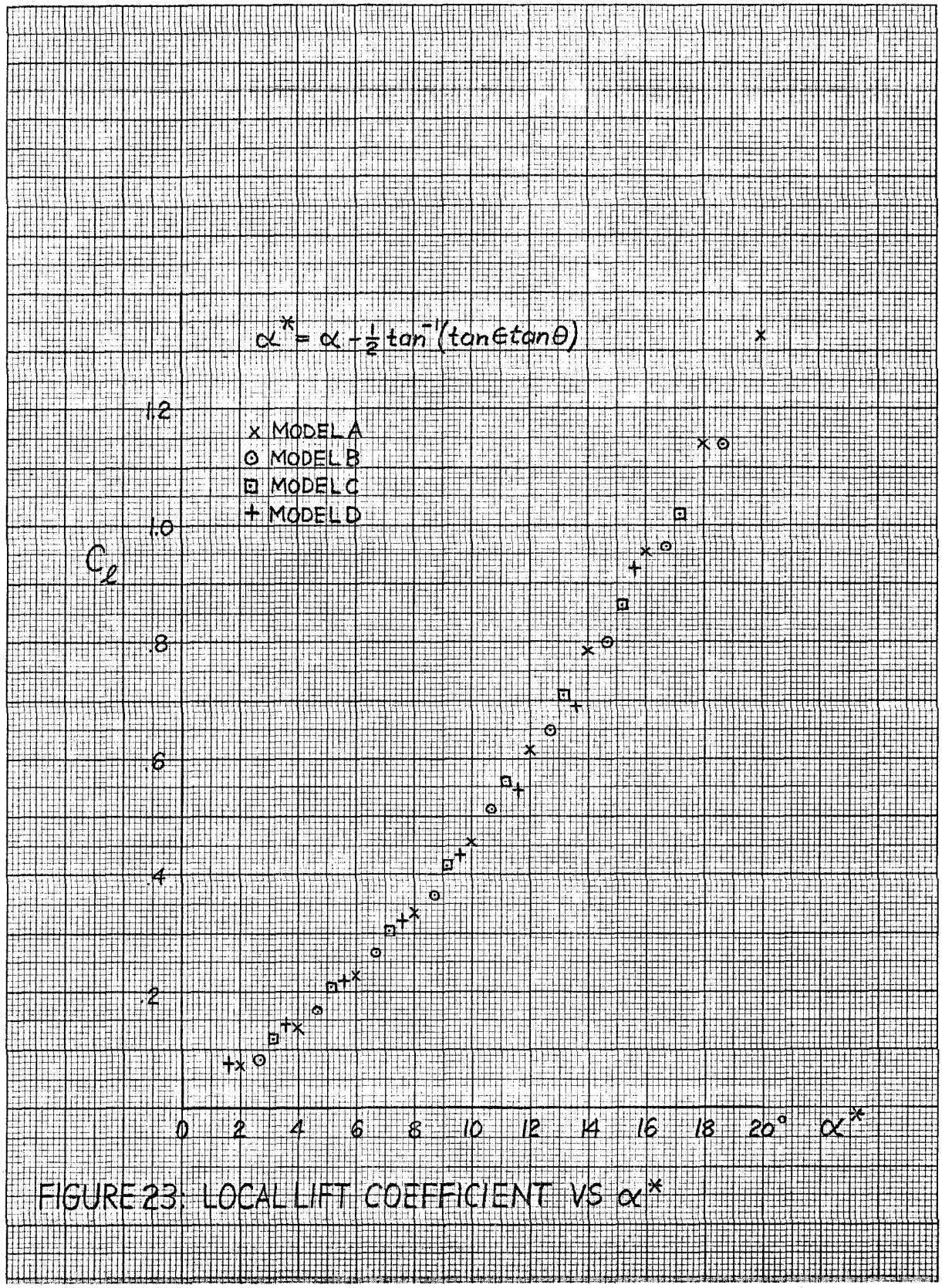

FIGURE 23: LOCAL LIFT COEFFICIENT VS α^*

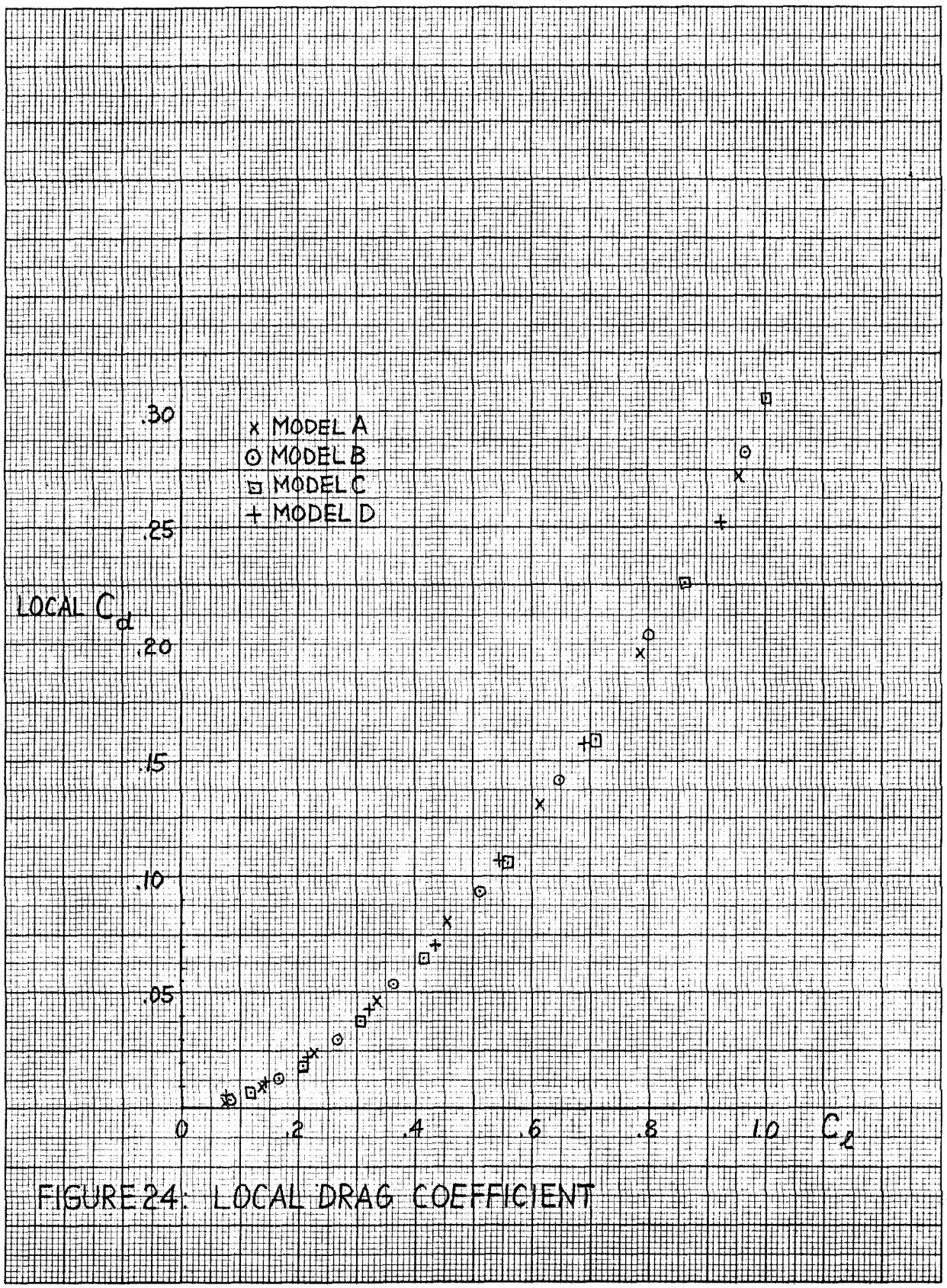

FIGURE 24: LOCAL DRAG COEFFICIENT

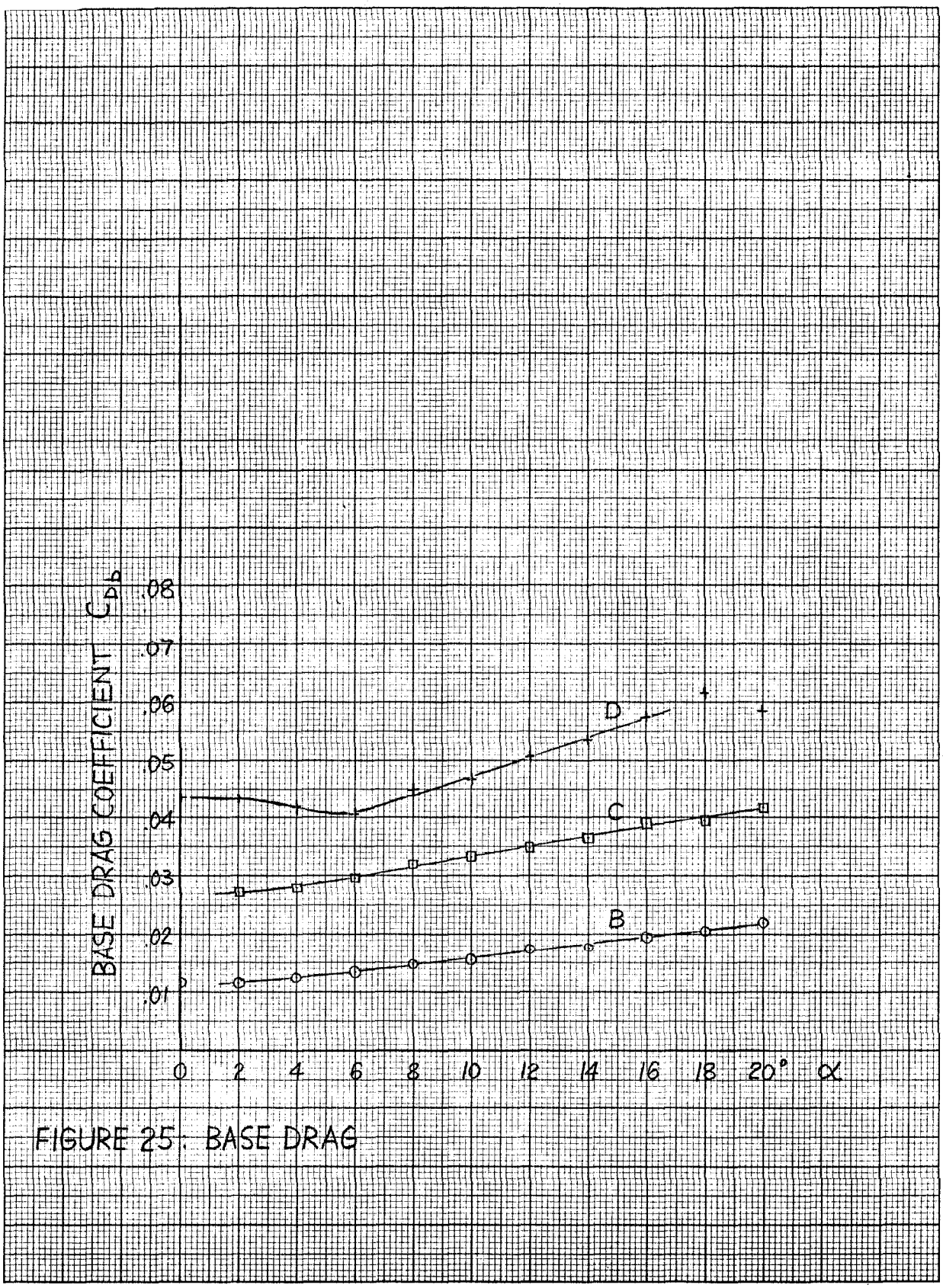

FIGURE 25. BASE DRAG

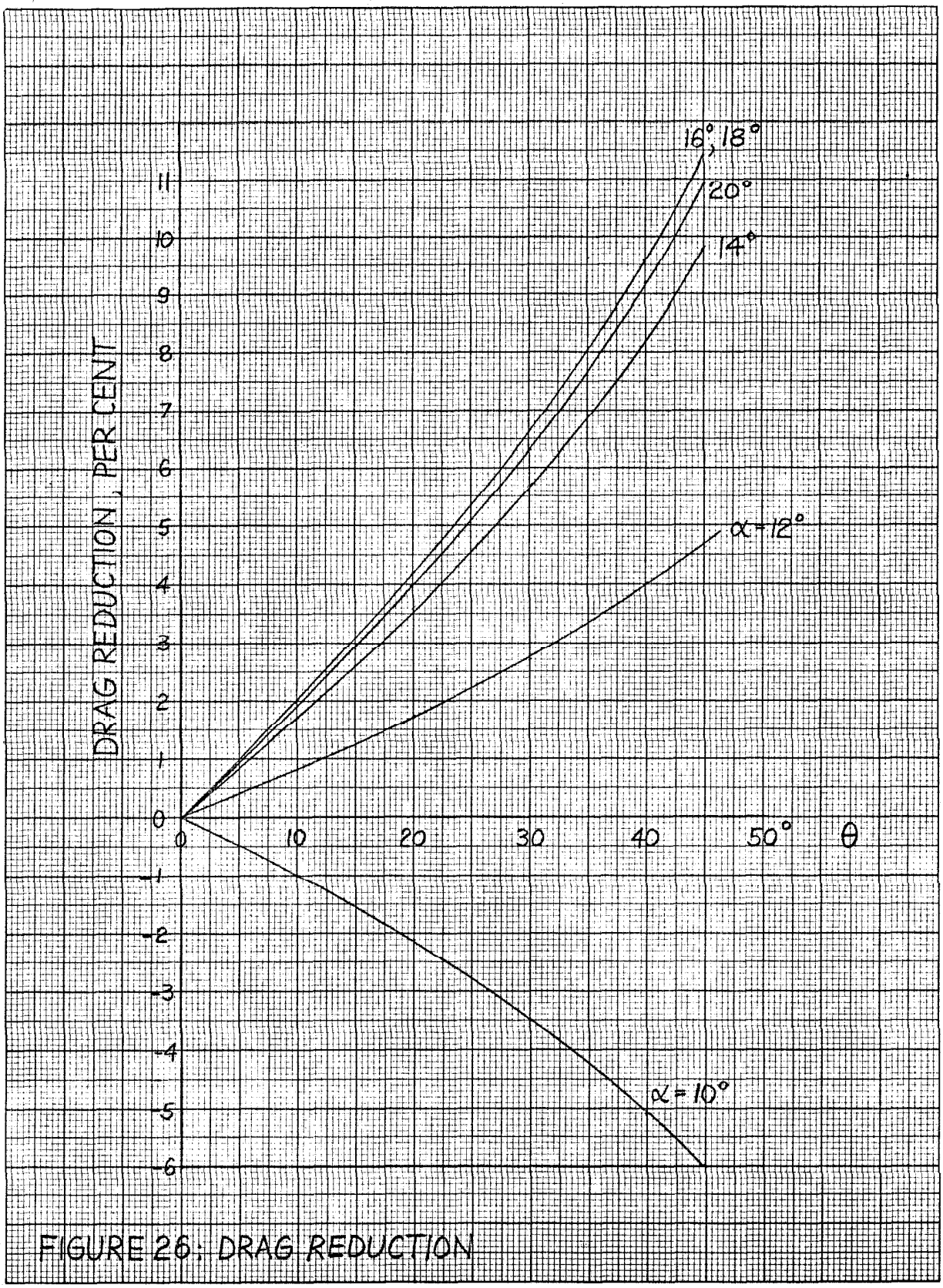

FIGURE 26: DRAG REDUCTION